POLITECNICO DI TORINO

Master's Degree in Biomedical Engineering

Politecnico di Torino

Master's Degree Thesis

Modeling the ECG and blood pressure time series of patients exposed to an external source of electromagnetic waves

Supervisors

Prof. J.A. TUSZYNSKI

Dr. Frederico COSTA

Candidate

Elizaveta LUGOVSKAYA

MARCH 2024

Abstract

Heart Rate Variability (HRV) is a measure of the variations in time intervals between consecutive heartbeats, reflecting the dynamic interplay between the sympathetic and parasympathetic branches of the autonomic nervous system. Beginning with an overview of the physiological basis of cardiac system, this master's thesis explores the most widespread technique to assess the heart rate variability, i.e., the ECG. Given that the patient data used to carry out the computational analysis derive from cancer patients, the research was carried out on the cardiac variability of people suffering from this disease and on new treatment option with exposure to low-energy amplitude-modulated radiofrequency electromagnetic fields. Moreover, this master's thesis investigated innovative methods for analyzing HRV data, including nonlinear dynamics, frequency-domain analysis, and time-domain measures.

There are several models that assess the cardiac variability. In the present study, the Van der Pol oscillator model has been selected to describe oscillations in a system with nonlinear damping. The Van der Pol heart model serves as a valuable tool for studying cardiac electrophysiology and understanding the mechanisms underlying heart rhythm disorders. Its ability to capture nonlinear dynamics and reproduce physiological phenomena makes it a useful framework for both theoretical analysis and computational simulations in cardiovascular research. The analysis of the parameter sensitivity of the solutions obtained from the Van der Pol model was carried out. It included the examination of changes of amplitude, frequency and shape through construction of time series graphs, phase maps and power spectrum plots. Then the analysis was done on the data of patients, which hemodynamic system was treated with external electromagnetic fields. The evaluation comprised time series, phase plots and recursive maps.

On the other hand, the Windkessel mathematical model has been used to explain how the cardiovascular system behaves, particularly the pulsatile blood flow in arteries. Mathematically, the Windkessel model can be described using differential equations that capture the relationships between pressure, flow, and volume within the arterial system. These equations can be solved to simulate various aspects of cardiovascular physiology, such as arterial pressure waveforms. The analysis of the blood pressure waves obtained from patient data, using phase maps and Poincaré maps was conducted.

Acknowledgements

I would like to express my sincere gratitude to my supervisor professor Jack A. Tuszynski for the opportunity he gave me and for his help during the development of the master's thesis and also to Dr. Frederico Perego Costa for providing me with patient data. I am thankful to my future husband Luca and for his family, in particular Anna and Valter, for always supporting me, especially in the most difficult moments. I would like to thank my mother Marina and her husband Valentin who, despite the distance that separates us, had the opportunity to be close to me. I am very happy to be surrounded by friends like Darya, Igor, Maria Grazia, Domenico and Massimiliano who have every time encouraged me in my studies. I am also enormously grateful to my colleagues Silvia, Simone and Martina who were present in times of need and always lent a hand.

Table of Contents

List of Tables

List of Figures

Acronyms

AD

Autonomic dysfunction

AHCC

Advanced hepatocellular carcinoma

ANS

Autonomic nervous system

AV

Atrioventricular

CEA

Carcinoembryonic antigen

CHB

Congenital heart block

DFA

Detrended fluctuation analysis

DTW

Dynamic time warping

ECG

Electrocardiogram

EMF

Electromagnetic fields

FF-ANNs

Forward artificial neural networks

FFT

Fast Fourier transform

GA

Genetic algorithm

HF

High frequency

HF-HRV

High-frequency spectral component of heart rate variability

HP

His-Purkinje

HR

Heart rate

HRV

Heart rate variability

IPA

Interiorpoint algorithm

LEAM

Low-energy amplitude-modulated

LF

Low frequency

MI

Myocardial infarction

MRBC

Metastatic and recurrent breast cancer

NN

Normal-to-normal

NN50

Number of successive intervals differing by more than 50 ms

NLD

Nonlinear dynamics

NMR

Nuclear magnetic resonance

ODE

Ordinary differential equation

PC-MRI

Phase contrast magnetic resonance imaging

pNN50

Percentage of successive intervals differing by more than 50 ms

PSA

Power spectral analysis

PSD

Power spectral density

RF

Radiofrequncy

RMSSD

Square root of the mean of squared differences between successive NN intervals

ROS

Reactive oxygen species

RT

Refraction time

SA

Sinoatrial

SDANN

Standard deviation of the averages of normal to normal beat intervals computed over 5-minute segments

SDNN

Standard deviation of normal to normal beat interval

TP

Total spectrum power

TSD

Time of spontaneous depolarization

TTD

Time-to-death

ULF

Ultra low frequency

VdP

Van der Pol

VEGF

Vascular endothelial growth factors

VLF

Very low frequency

Chapter 1

Heart Rate Variability

1.1 Heart anatomy and cardiac cycle

The heart is a specialized pump that pumps blood throughout the body by contracting repeatedly and regularly. The heart in humans, other mammals, and birds has four compartments: two atria and two ventricles. An intricate web of self-excitatory components can be used to understand how the electrical impulse conduction in the heart system occurs. The natural pacemaker, the SA node, experiences the first stimulation, which spreads like a wave and stimulates the atria. Made primarily of cells known as pacemaker cells, the sinoatrial node is an oval-shaped area of unique cardiac muscle at the upper back wall of the right atrium (Figure 1.1). To coordinate the heart's upper chamber beating, the atrioventricular node electrically joins the ventricles and atria. When the stimulus gets to the AV node, it starts a pulse that first activates the His bundle and then the Purkinje fibers. The bundle of His is a group of heart muscle cells with electrical conduction functions. It is a component of the heart's electrical conduction system and carries electrical impulses from the atrioventricular node to the bundle branches, which mark the apex of the fascicular branches. The Purkinje fibers, which supply electrical conduction to the ventricles and cause its heart muscle to contract at regular intervals, are the next structure that the fascicular branches lead to.

The contracting and relaxing of the cardiac muscles produce the heartbeat. The contraction phase of this cycle is known as systole, while the relaxation phase is known as diastole. A person blood pressure drops when their heart relaxes and fills with blood; on the other hand, when the heart contracts, blood is forced out of the heart and into the big blood arteries that make up the circulatory system. The blood then travels to all the body's tissues and organs. The first phase of the heart cycle is atrial diastole. It happens a few milliseconds before the atria get the electrical signal from the SA node. Blood pools in the atria during the early stages

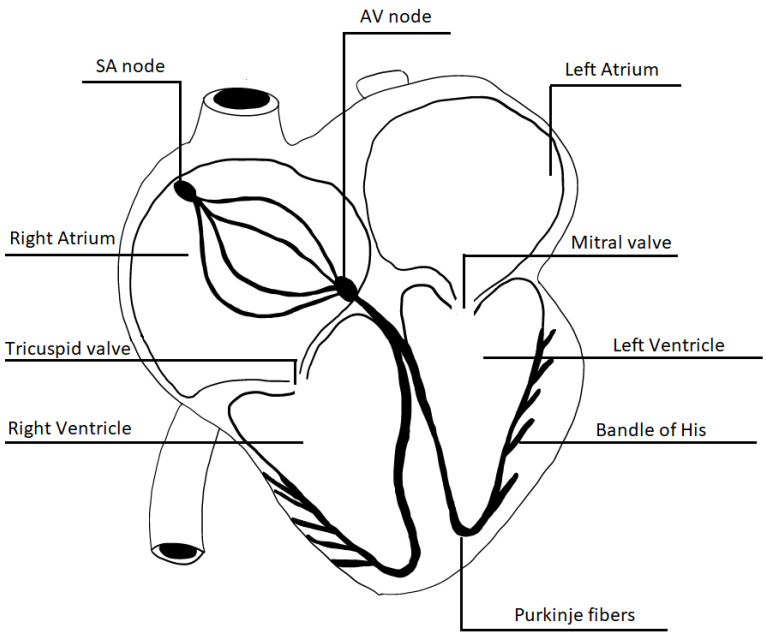

Figure 1.1: Heart anatomy

of this phase when the atrioventricular valves are closed. There is a moment at which the pressure in the atrium is higher than the pressure in the side ventricle. Blood can enter the ventricle because of the pressure difference that opens the atrioventricular valves. An action potential is started by the autonomous sinoatrial node and spreads throughout the atrial myocardium. Any blood that remains in the upper chambers of the heart is forced into the lower chambers by the concomitant contraction of the atria brought on by the electrical depolarization. The semilunar and atrioventricular valves are closed in the early phases of ventricular diastole. The volume of blood in the ventricle does not vary throughout this phase, but the intraventricular pressure drops sharply. This is known as isovolumetric relaxation. The atrioventricular valves open when the ventricular pressure eventually drops below the atrial pressure. This causes the ventricles to rapidly fill with blood. The atria depolarize just before the electrical impulse reaches the atrioventricular node. The ventricles are not depolarized until the atria have finished contracting due to a little delay at the AV node. The action potential travels via the His bundle and then the left and right bundle branches. Ventricular contraction is caused by the electrical impulses that these fibers carry through the corresponding ventricular regions. The semilunar valves open to let blood exit the ventricle when the pressure

inside the ventricle rises above the pressure in the outflow tube. The cardiac cycle's ejection phase is currently underway.

1.2 ECG

The electrical current that cycles through the heart and propels its pumping action is known as heart rate (HR) or heart pulse. The heart rate is determined by counting the number of contractions in a given amount of time. According to certain theories, heart rate variability (HRV) is a crucial technique for evaluating cardiovascular autonomic characteristics that are largely regulated by innervations from the sympathetic and parasympathetic nervous systems [1]. In general, HRV is regarded as a measure of regulatory influences, primarily of the activity of the ANS (Autonomic Nervous System) to control cardiovascular system function [2]. Previous research has shown that HRV may be used to distinguish between healthy and diseased states because the vagal-mediated HRV indices showed an inverse relationship with a number of risk variables for diabetes, insulin resistance, glucose intolerance, central obesity, dyslipidemia, and hypertension [3].

Many sophisticated techniques can be used to assess HRV. With consideration for the temporal variance between successive heartbeat sequences, the conventional ECG method is the most often used approach. The heart's electrical activity is recorded by the electrocardiogram (ECG), which is helpful in analyzing the heart's behavior and determining the frequency and regularity of heartbeats. The non-invasive nature of ECG has led to its extensive application. In essence, the electrical pulses produced by heart activity are captured as waves that represent the electrical current flowing through various heart regions. It is crucial to highlight three key elements in the normal cardiac cycle: P wave, QRS complex and T wave (Figure 1.2).

A steady R-R space is seen in the normal state, with the P wave forming before each QRS complex, which in turn needs to occur before each T wave. The impulse produced by the SA node is represented by the P wave. The P wave causes the atria to compress and depolarize during normal electrical activity. Its amplitude is smaller than 2 mm, and its period ranges from 0.08 to 0.1 s. The QRS complex is responsible for the depolarization and contraction of the ventricles. The interval ranges from 0.12 to 0.20 s between the P wave's beginning and the QRS complex. This duration, which is equivalent to the PR or PQ interval, shows how long it takes an electrical impulse to move from the sinus node to the ventricles via the atria. When there is a higher rhythm, the PR interval gets smaller. Ventricular repolarization, which occurs when heart cells get back to being prepared to respond to a different stimulus, is reflected in the T wave.

While a normal ECG appears to be periodic, heart rate variability, which is

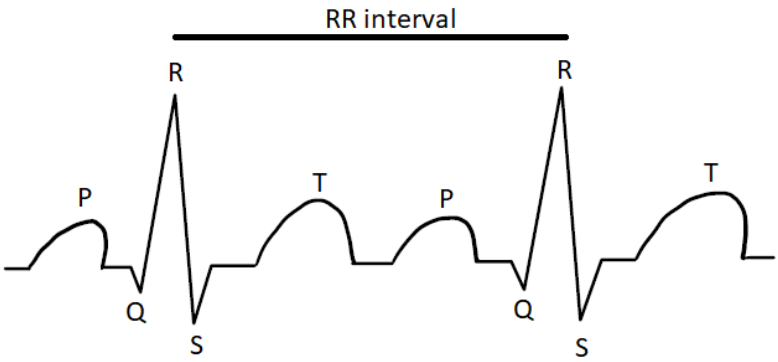

Figure 1.2: ECG response representing a normal cardiac cycle characterized by three important components: P wave, QRS complex and T wave.

quantifiable based on R-R intervals, is typically present [4]. Depending on the level of activity, disruptions may cause an increase or decrease in rhythm that results in arrhythmias. Short-term (2–5 minutes) or long-term (24–48 hours) ECG recordings can be used to calculate HRV. Although there are other ways to quantify it, the traditional time domain (statistical and geometrical) and frequency domain (power spectral density) measuring approaches are still widely used [5]. Numerous physiological and pathological circumstances have an impact on HRV. There are several pathophysiologic illnesses that have been linked to a loss or reduction in beat-to-beat interval variability such as myocardial infarction, ventricular arrhythmias, congestive heart failure and etc [6]. Not only are heart ailments associated with significantly altered HRV present, but a wide range of pathophysiologic disorders marked by neurohumoral activation also exhibit this feature [7].

1.3 Hypothesized prognostic role of HRV in cancer

HRV could be a helpful non-invasive method for assessing cancer patient prognosis as well as being a predictor of unfavorable outcomes in congestive heart failure, myocardial infarction, sudden cardiac death and also as an early indication for diabetic neuropathy [8]. According to most studies, people with cancer frequently have a lower heart rate, which is probably due to autonomic dysfunction brought on by the illness [8],[9],[10]. The fundamental theory holds that there are three pathways via which a decreased HRV is linked to tumor growth: oxidative stress, inflammation, and sympathetic nerve activation. Oxidative stress causes unchecked

cell proliferation as well as DNA damage, which is a major cause of tumorigenesis. In the early phases of oncogenesis, localized hyperinflammatory responses encourage tumorigenesis; in the later stages, they facilitate disease progression. Normally enlisted to aid in the fight against and removal of malignancies, the inflammatory milieu is inadvertently fueling the growth of the tumor and generating free radicals to worsen oxidative stress. Ultimately, sympathetic neurotransmitters, such as norepinephrine, regulate the metastatic process by enhancing cancer cells' ability to migrate and directing the growth and direction of metastases [11].

Heart rate variability, which is a biomarker of autonomic nervous system function, quantifies the ANS by altering cardiac function in a sympathetic and parasympathetic manner. The primary modulator of the parasympathetic innervation of the heart and the principal constituent of the parasympathetic nervous system is the vagal nerve. HRV is an important non-invasive index of vagal nerve activity. Recent research has started looking into how vagal nerve activity is related to cancer prognosis. Giese-Davis et al.(2015) discovered that among women diagnosed with metastatic and recurrent breast cancer (MRBC), higher resting high-frequency spectral component of heart rate variability (HF-HRV) substantially predicted longer overall survival [12]. This discovery may be mediated by behavioral characteristics that affect vagal activity and lengthen cancer survival, such as emotional expressiveness, social support and involvement, adherence to therapy, and reduced levels of depression. Reduced vagal activity, increased sympathetic activity, or a combination of these largely independent autonomic circuits can all lead to increases in heart rate. A study by Couck et al. (2012) found that all three main mechanisms (oxidative stress, inflammation and sympathetic nerve activation), as well the cancer themselve, are inversely correlated with efferent vagal activity, which may be non-invasively assessed by HRV and suggested that vagal activity may mitigate the impact of risk factors on the onset of cancer [8]. In the study of Couck et al. (2013) the effect of cancer severity on vagal nerve activity, indexed by HRV, was investigated combining data of five different cancers (colorectal, pancreas, prostate, lung and ovarian) [9]. It was found that patients heart rates were considerably greater in the early stages than in the later stages, while age and gender did not significantly affect HRV. This could mean that disease severity influences HRV. The explanation for this discovery could be the fact that during the metastatic stage oxidative stress, inflammation and sympathetic nerve activation might have a bigger impact on HRV or that treatments (e.g. chemotherapy) reduce vagal nerve activity. The entire HRV, comprising the short- and long-term components that cause fluctuations during the recording period, is reflected in the SDNN. The study of Mouton et al. (2012) examined the connection between carcinoembryonic antigen (CEA) levels, a vagal nerve measure, and baseline HRV (SDNN) [10]. The acquired results corroborate the neuromodulatory involvement of the vagus nerve in cancer prognosis and the postulated prognostic role of HRV in cancer.

For cancer patients, accurate survival estimation is crucial, particularly in cases where there is little chance of a cure. Improved time-to-death (TTD) prediction can help with planning and decision-making for successful end-of-life care for patients in hospice units. In some released works it has been hypothesized that in cancer patients, autonomic dysfunction (AD) as assessed by HRV is linked to a poor prognosis for survival [13],[14],[15],[16]. In the work published by Fadul et al. (2010) a strong correlation between time domain measure of standard deviation of normal to normal beat interval (SDNN) and survival in male patients with advanced cancer was discovered [13]. Also the study conducted bu Guo et al. (2015) demonstrated that a lower HRV is linked to a shorter survival time [14]. Kim et al. (2010) investigated how well HRV measures could forecast the length of survival for terminally ill cancer patients [15]. According to the investigation's findings, most terminal cancer patients have impaired HRV, and SDNN may be able to help these patients anticipate how long their survival will be. In the study of Chiang et al. (2010) the frequency-domain analysis of HRV was conducted [16]. It was demonstrated that in individuals with terminal hepatocellular carcinoma, elevated total spectrum power (TP) was substantially correlated with longer TTD. These results confirm the hypothesis that prognostic models including HRV monitoring may predict TTD more accurately and in this way help doctors make better decisions when treating hospice patients.

It is unclear exactly whatever processes underlie the association between HRV and the prognosis for cancer. Nonetheless, it's believed that HRV could be a sign of general health and physiological toughness. A drop in HRV could be a sign of a decline in physiological resilience, which could make it harder for cancer patients to withstand treatment and overcome their illness.

1.4 Exposure to low-energy amplitude-modulated radiofrequency electromagnetic fields

Various studies deal with the detection of the effects of low frequency electromagnetic fields on tumor proliferation and cell differentiation, quantification of the latency times between irradiation and biological effects and indications on the cellular mechanisms underlying the effects detected. In the work of Tuszynski et al. (2022) the mechanism of action of the exposure to low-energy amplitude-modulated radiofrequency electromagnetic fields (LEAM RF EMF) for patients with advanced hepatocellular carcinoma (AHCC) was analysed [17]. In this study [17] a medical device with a carrier wave frequency of 27.12 MHz is utilized, the device can detect changes in a patient hemodynamic parameters related to a particular health condition when the patient is exposed to low-energy, amplitude modulated electromagnetic field frequencies. The customized or tumor-specific envelope wave

frequencies utilized are in the range between 10 Hz and 150 kHz [18]. In vitro these particular frequencies slowed the growth of human cancer cell types without having thermal effects on tissue. The exposure to LEAM RF EMF in clinical studies is provided via an intrabuccal antenna (Figure 1.3).

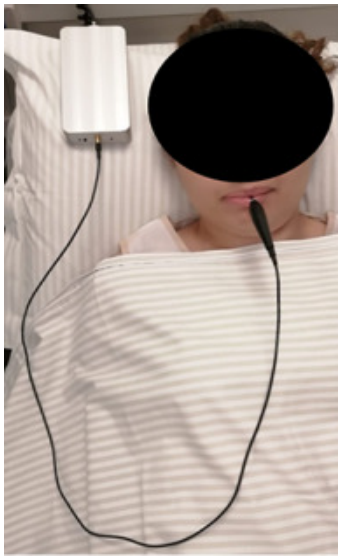

Figure 1.3: Patient undergoing the procedure showing the medical device and intrabuccal spoon-shaped antenna [19].

One way to conceptualize carcinogenesis is as a phase shift whereby typically homogeneous, synchronized, and differentiated cells in ordered tissues give way to asynchronized, heterogeneous, dedifferentiated, and proliferative cancer cells in disordered tumors [20]. Research suggests that compared to normal cells, cancer cells may be more sensitive to EMF disruption. High electrical dipole moment molecules and ions are vulnerable to frequency-dependent interactions with electromagnetic fields [21]. Thus, EMFs apply strong dielectrophoretic pressures on microtubules, potentially impairing cell division. Microtubles, actin filaments, collagen and DNA are all elongated polymeric structures with high electric charges, allowing them to carry electrical currents through the surrounding counterions. This characteristic renders them possible candidates for resonant interactions with LEAM RF EMFs. Microtubules are considered as the primary cellular bio-antenna for therapeutic LEAM RF EMFs because of their notably high electric charge and dipole moment values, which allow for direct coupling with EMFs [17].

Chapter 2

Mathematical models of HRV

2.1 HRV measures

As mentioned before, the main measures of HRV are time-domain and frequency-domain. Time-domain measures quantify the variability of the HR over various time intervals and are expressed in milliseconds. If the time-domain analysis is performed directly on the normal-to-normal (NN) intervals, the measures like standard deviation of all NN intervals (SDNN) and standard deviation of the averages of NN intervals computed over 5-minute segments (SDANN) could be obtained. If the time-domain analysis is carried out on the differences between successive NN intervals, as a result the values of RMSSD (square root of the mean of squared differences between successive NN intervals), NN50 (number of successive intervals differing by more than 50 ms) or pNN50 (percentage of successive intervals differing by more than 50 ms) could be calculated [22]. Frequency-domain measurements, which are reported as power, correlate to oscillations of the HR throughout a variety of particular frequencies, including low frequency (LF), high frequency (HF), very low frequency (VLF), and ultra low frequency (ULF). Since they need to convert a signal from the time domain to the frequency domain, they demand more advanced conceptual and computational understanding. The LF is linked to the regulation of blood pressure and is a sign of sympathetic activity. Respiratory sinus arrhythmia, which is indicative of parasympathetic activity, is connected with HF. Temperature control or vasomotor control are connected to the VLF [23]. The power spectrum consists of a very low frequency peak below 0.05 Hz, a high frequency peak between 0.15 Hz and 0.4 Hz, and a low frequency peak between 0.06 Hz and 0.15 Hz. Power spectral analysis (PSA), which enables the RR interval series to be mathematically decomposed into components of various

frequencies, is used to go from the time to the frequency-domain. The fast Fourier transform (FFT) and autoregressive modeling are the two most widely used methods for PSA.

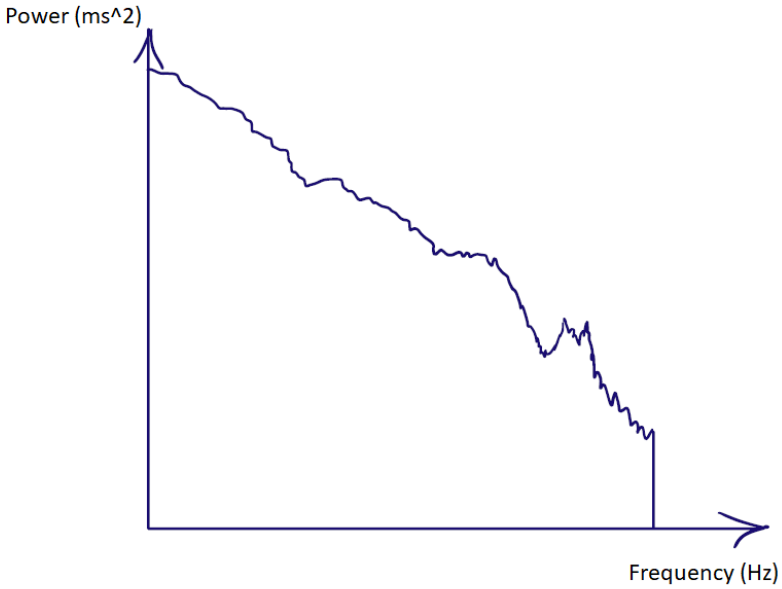

Figure 2.1: Exponential increase in power as frequency decreases in normal sinus rhythm.

In addition to measurements in the time and frequency domain, there are nonlinear measurements. Nonlinear HRV measurements aim to quantify the structure or complexity of the RR interval time series, while time and frequency domain measures of HRV quantify HRV on different time scales. The analysis of nonlinear systems is best suited for nonlinear measurements. Only a small fraction of the several nonlinear HRV measurements that have been researched, have demonstrated a definite benefit in risk categorization. These consist of the SD12 measure, which is derived from Poincare plots, the power law slope, and the exponent of both short- and long-term fractal scaling. Spectral power shows a progressive, exponential decrease in amplitude with increasing frequency in normal sinus rhythm (Figure 2.1). An alternative way to represent this relationship is as the log of power (Y axis) against the log of frequency (X axis), which converts the exponential curve into a line with an approximated slope (Figure 2.2). Derived from PSA, the power law slope evaluates complexity in the longer term (minutes to hours). The beta (β) index represents the negative slope of the log-power against log-frequency line in the ULF-VLF region, which lies between 10^2 and 10^4 Hz. A steeper line corresponds to a lower β and a larger loss of complexity. Reduced power law It has

been demonstrated that slope is a predictor of an elevated mortality risk following myocardial infarction (MI) [24]. Detrended fractal scaling exponent measures complexity in the shorter period (3–20 beats). This measure is computed from detrended fluctuation analysis (DFA). The positive slope is represented by the alpha (α) index, which is further split into two indices, α_1 and α_2, that represent the fractal characteristics of HRV over various time scales. The intermediate-term scaling exponent (12-20 beats) is represented by α_2, whereas the short-term scaling exponent (3-11 beats) is denoted by α_1 [25]. On a scale of three to eleven beats, α_1 represents how random or coupled the R-R interval pattern is at one extreme. A completely random RR interval pattern has an α_1 value of 0.5, whereas a completely correlated, or perfectly periodic, pattern of R-R intervals has a value of 1.5. Reduced α_1 readings are highly indicative of the outcome following a MI [26]. The α indices typically have values near 1, and both larger and lower values signify a loss of complexity. Every RR interval is plotted on the Poincaré graph as a function of the subsequent RR interval. The recurrence plot is a commonly employed visual aid for identifying oscillations in non-linear dynamic systems. Fitting an ellipse to the Poincaré plot yields SD12. This ellipse has two axes: SD1 is its short axis and SD2 is its long axis. SD12 is their ratio. The complexity of the figure increases with the relative magnitude of SD1 over SD2, and SD12 grows larger. SD12 has shown promise in identifying editing issues that have a substantial impact on the HRV variable computation.

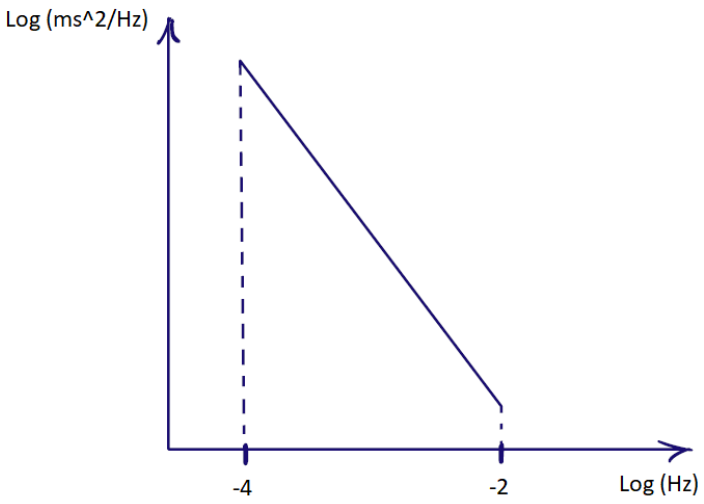

Figure 2.2: Log-power with β slope.

The most famous example of nonlinear behavior is chaos; technically, it is

actually "deterministic chaos," but in mathematics, chaos refers to a behavior that is only seemingly erratic because it can be predicted by complex mathematical equations, despite the term being used colloquially to denote complete randomness. Chaos is a term used to describe an apparently random kind of variability that can occur when even the simplest non-linear system functions. The behavioral analysis of dynamical systems that show sensitivity to initial conditions is the foundation of chaos theory. According to this hypothesis, little variations, such as those resulting from rounding errors in numerical calculations, produce divergent results. Long-term, this causes dynamical systems to become unpredictable.

2.2 Van der Pol equations and mathematical modeling

Originally, the theory of nonlinear dynamics (NLD), which emerged in the late 1970s and early 1980s, attracted the attention of numerous scientists who wanted to investigate chaotic behavior in biological systems and use the results to advance biology and medicine. Subsequently, the emphasis switched to the apparently high dimensional cardiovascular system, with an explanation and accounting for nonlinearity. Currently, identifying and characterizing the complexity and dynamics of nonlinear systems is a popular strategy. When a system is nonlinear, its variables contribute to the output response rather of producing it as in a linear system. Given that the input stimulus and the initial conditions of all variables affect the output response, even a slight modification can have a significant impact on a nonlinear system. In order to model HRV using nonlinear differential equations, mathematical models of the ANS's dynamics and interactions with the cardiovascular system must be used.

The modelling of HRV could be explored using a particular nonlinear differential equation called "Van der Pol Equation". The van der Pol (VdP) equation is a second-order differential equation that describes the behaviour of a nonlinear oscillator. The VdP system has been widely used in theoretical models of the heart rhythm since it was first introduced to describe relaxation oscillators in electrical circuit modeling. Relaxation oscillators generate a nonsinusoidal repeated output signal through a nonlinear electronic oscillator circuit. Two alternating processes operating on distinct time scales are distinguishing features of relaxation oscillations: a long relaxation period that sees the system get closer to equilibrium, interspersed by brief impulsive period that causes the equilibrium point to shift. Their waveform is far from sinusoidal, and prominent amplitude higher harmonics are present in large numbers as steep portions occur [27]. Here is the sort of nonlinear oscillator model that represents the heart mathematically using the VdP

system:

$$\ddot{x} + \alpha(x^2 - 1)\dot{x} + \omega x = 0 \tag{2.1}$$

where α and ω are related to damping and Duffing parameters of the system. An essential component of a cardiac pacemaker is the VdP equation's ability to adjust its inherent frequency to the external driving pacemaker frequency without affecting amplitude. Grudzinski and Zebrowski introduced these traditional VdP heart models [27]. To derive the equation (2.1) the electrical RLC circuit must be considered that consists of an inductance L, a capacitor C, a resistor R and the voltage source E(t) [28]. Kirchhoff's Voltage Law states that a current I(t) starts to flow in the circuit when the battery switch is closed:

$$L\dot{I} + RI + \frac{1}{C}Q = E \tag{2.2}$$

where Q is the charge of the capacitor and $\dot{Q}$=I. When the equation (2.2) is derived, we obtain a damped harmonic oscillator represented by a second-order linear ordinary differential equation (ODE) with constant coefficients:

$$L\ddot{I} + R\dot{I} + \frac{1}{C}I = 0 \tag{2.3}$$

Nevertheless, Van der Pol's circuit showed an active element—a semiconductor array of vacuum tubes—instead of a passive resistor (Figure 2.3). In this manner, when the current is low, the semiconductor functions as though it is pumping energy into the system, and when the current is too large, it damps the energy of the system. The function I^2-α, where α is the current threshold, models the semiconductor's action. After this consideration, the equation becomes:

$$L\dot{I} + (I^2 - \alpha)I + \frac{1}{C}Q = E \tag{2.4}$$

If the equation (2.4) is derived, it becomes:

$$L\ddot{I} + 3\dot{I}(I^2 - \frac{\alpha}{3}) + \frac{1}{C}I = 0 \tag{2.5}$$

The VdP equation can be represented in standard form (2.1) by rescaling the constants of the equation (2.5).

Later on, the saddle and stable node fixed points at x = -d and x = -2d, respectively, significantly altered the features of the original classical VdP heart model. In light of this, the VdP system for the heart model with revised unsymmetrical damping terms associated with voltage is as follows:

$$\ddot{x} + \alpha(x^2 - \mu)\dot{x} + \frac{x(x+d)(x+2d)}{d^2} = 0 \tag{2.6}$$

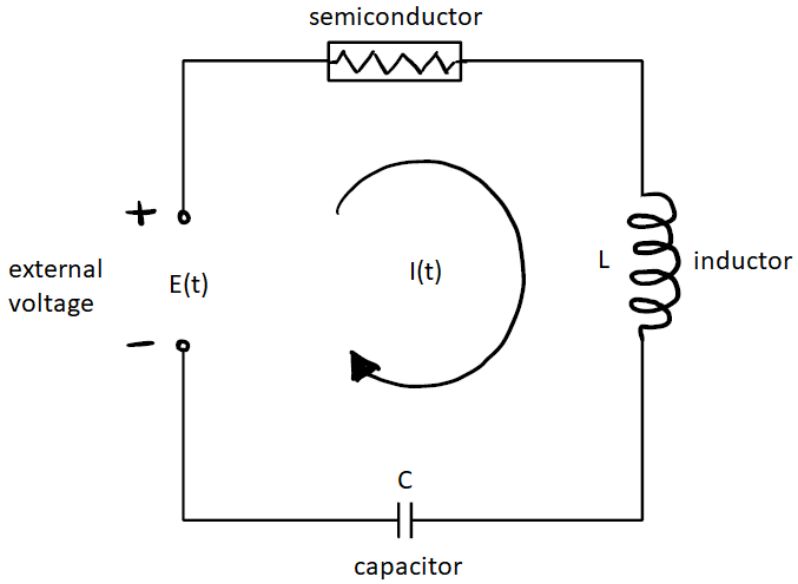

Figure 2.3: Van der Pol oscillator with external voltage E(t), semiconductor, inductor L, capacitor C and current I(t).

Then the system (2.6) is modified by the introduction of a new parameter e, responsible for the change in depolarization period:

$$\ddot{x} + \alpha(x^2 - \mu)\dot{x} + \frac{x(x+d)(x+e)}{ed} = 0 \tag{2.7}$$

The damping term $\alpha(x^2 - \mu)$ was further updated in Equation (2.7) by substituting it with $(x-\nu_1)(x-\nu_2)$:

$$\ddot{x} + \alpha(x - \nu_1)(x - \nu_2)\dot{x} + \frac{x(x+d)(x+e)}{ed} = 0 \tag{2.8}$$

For the system to continue having its self-oscillatory properties, the condition $\nu_1\nu_2<0$ must be met. Moreover, the novel model can replicate the fundamental physiological characteristics of an average cardiac pacemaker. In the event that system (2.8) is updated as follows in response to an external pacemaker or forcing factor F(t):

$$\ddot{x} + \alpha(x - \nu_1)(x - \nu_2)\dot{x} + \frac{x(x+d)(x+e)}{ed} = F(t) \tag{2.9}$$

In order to investigate the characteristics of cardiac rhythm, the nonlinear Van der Pol oscillator-based model of the heart is presented in equation (2.9). In the system

(2.9) variables x and α represent the length of the heart fiber and the factor used to modify the pulse shape of heartbeat, ν_1 and ν_2 represent the parameters that make up the asymmetric term that changes the damping term in the classic VdP equation, e denotes the ventricular contraction period, d is a factor that arises to replace the harmonic forcing in the classic VdP equation by a cubic term, and F(t) is the external forcing factor [29]. A well-posed problem with a singular solution is formulated by two initial conditions:

$$x(0) = c_1 \tag{2.10}$$

$$\dot{x}(0) = c_2 \tag{2.11}$$

As was previously noted, the SA node—which is regarded as the normal pacemaker—is principally responsible for producing the regular heart rhythm. Furthermore, an additional pacemaker is the AV node. An essential component of the mechanics of the heart is presented by each of these actuation potentials. Because each activation—depolarization followed by repolarization—corresponds to a distinct cardiac area, it produces currents that vary in strength. The ECG is therefore the result of the combination of activation waves originating from each area of the heart; certain signals, such as those originating from the atrium and ventricle, may predominate in this composition. Based on these suppositions, the general heartbeat dynamics may be represented by connected oscillators, each of which represents a distinct heart area signal. Typically, the SA and AV nodes are represented by two oscillators; however, it has been found that these oscillators are insufficient to replicate the ECG signal. This is due to the fact that the first oscillator's signal is associated with the atrium and SA node activity, whereas the second oscillator's signal is solely associated with the ventricle depolarization. As this time primarily corresponds to the ventricular repolarization, it is conceivable to reconstruct the P-curve but not the QRS complex under this premise. This finding led to the addition of a third oscillator to simulate the pulse propagation via the ventricles. This oscillator physiologically replicates the His-Purkinje (HP) complex, which is made up of the Purkinje fibers and the His bundle. All oscillators are assumed to have bidirectional asymmetric couplings in order to construct a broad model (Figure 2.4).

2.3 Lyapunov exponent and Poincaré plot

The dynamics perspective is an intriguing method for determining cardiac rhythms, and the type of dynamic response is useful information in this context. The average exponential rates at which neighboring orbits diverge or converge in phase space are known as Lyapunov exponents [30]. Exponential orbital divergence indicates that systems whose beginning differences we may not be able to resolve will soon

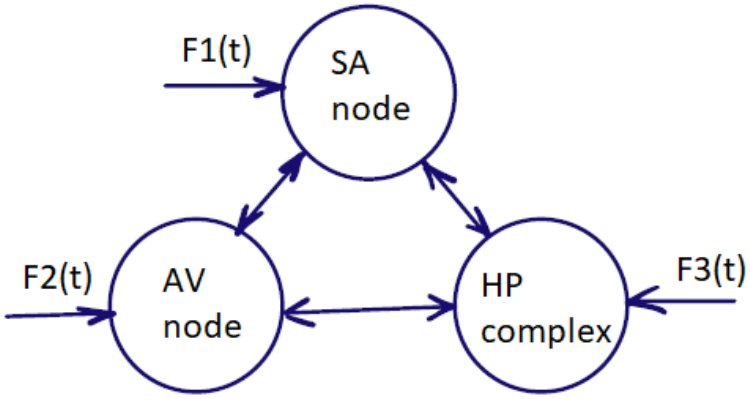

Figure 2.4: General model with three coupled oscillators: sinoatrial node, atrioventricular node and His-Purkinje complex.

act substantially differently—predictive capacity is rapidly lost. This is because neighboring orbits correspond to nearly identical states. When studying a dynamic system, the maximal Lyapunov exponent is typically evaluated in order to obtain the most information possible. It is crucial to determine Lyapunov exponents in order to recognize the chaotic behavior of cardiac systems [31]. It is a curve that displays a great deal of dynamic behaviors, many of which are unknown. Among these data, a positive maximum Lyapunov exponent serves as an illustration of the chaotic nature. The evolution of minor disturbances to the system during its time evolution can be carried out by calculating a maximal Lyapunov exponent. Therefore, at the distance between initially neighboring points, there is a stretch for a positive maximal Lyapunov exponent, and this is chaos. A system is considered chaotic if it has at least one positive Lyapunov exponent, and the exponent's magnitude indicates the time scale at which the dynamics of the system become unpredictable [32]. Additionally, there is a contraction or approach for a negative exponent that is characteristic of a particular oscillatory or static condition; this is regularity. Lastly, for a zero exponent, we get a collection of quasiperiodic waveforms, which include the torus in certain instances [33].

Considering two points in a space, x_0 and $x_0+\triangle x_0$, each of which will generate an orbit in that space (Figure 2.5), the mean exponential rate of divergence of two initially closed orbits becomes:

$$\lambda = \lim_{t\to\infty} \frac{1}{t} \ln\left(\frac{\triangle x(x_0,t)}{|\triangle x_0|}\right) \tag{2.12}$$

The distance between the two orbits will depend on time if one of them is utilized

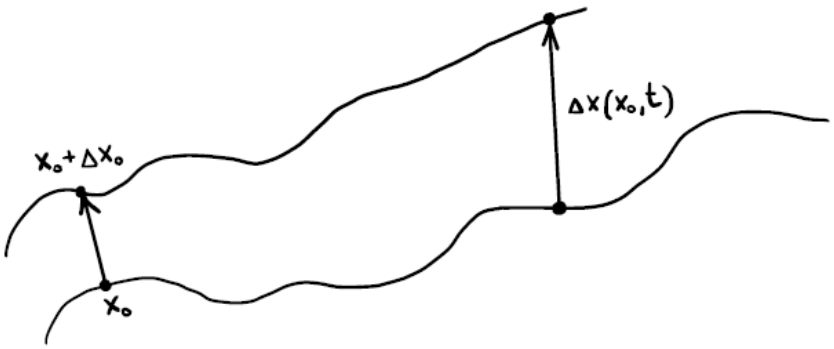

Figure 2.5: Two neighbouring trajectories.

as a reference orbit. Since sensitive dependency can only occur in specific areas of a system, this separation takes the form of a location function of the initial value and becomes $\triangle x(x_0, t)$ [34]. The function $\triangle x(x_0, t)$ will exhibit unpredictable behavior during chaotic areas. Chaotic signal pathways in state-space exhibit conventional patterns. Trajectories that are closely spaced from one another converge and diverge exponentially. If the exponent is negative (λ <0) the orbit attracts a stable fixed point or stable periodic orbit. Dissipative or non-conservative systems are characterized by negative Lyapunov exponents. The stability increases with the exponent's negative value. The Lyapunov exponent of super stable periodic points and fixed points is λ =-∞. In case if the exponent is equal to zero the orbit is a neutral fixed point. When the system has a zero Lyapunov exponent, it is in a steady state mode. This exponent indicates that the physical system is conservative. In conclusion, the orbits are on a chaotic attractor if the exponent is positive. Any arbitrary gap will cause nearby points to diverge, regardless of how close they are. These points are unstable. The largest Lyapunov exponent provides a prediction metric that quantifies the system's sensitivity to initial conditions. Congenital heart block (CHB) and ischemic/dilated cardiomyopathy are examples of slowly varying signals where this value decreases; in the other situations, where RR variation is greater, the value will be higher [34].

Poincaré map is a nonlinear tool with the function of rhythm identification and diagnosis purposes. The pathological features are highlighted using the Poincaré map. It makes it possible to comprehend the global system dynamics better by condensing the time continuous dynamics into a discrete set of states, or a map [31]. Return map is one of the approach to build the Poincaré map. It constructs a Poincaré map by taking into account sequential trajectory junctions with a subsapace hypersurface [31]. In a highly simple phase space, also known as a cartesian plane, the values of each pair of subsequent components in a time

series are visually represented. A Poincaré plot is a graphical representation that displays the correlation RR_{n+1} as a function of RR_n, where R represents the peak of the QRS complex for each beat in the ECG signal and RR_i is the beat-to-beat interval [35]. A curve, or trajectory, that depicts the system's evolution is formed by a sequence of these points at different intervals, and is thus frequently used to evaluate the dynamics of heart rate variability. Poincaré plot analysis is a developing quantitative-visual technique that divides the plot's form into functional groups that represent the severity of a subject's heart failure. The quantitative analysis of HRV by transforming the Poincaré plot into an ellipse, has been already discussed in chapter 2.1. Three indexes are obtained with this technique: the axis ratio (SD1/SD2), the standard deviation of the continuous long-term RR interval variability (major axis of the ellipse or SD2), and the standard deviation of the instantaneous beat-to-beat RR interval variability (minor axis of the ellipse or SD1) (Figure 2.6).

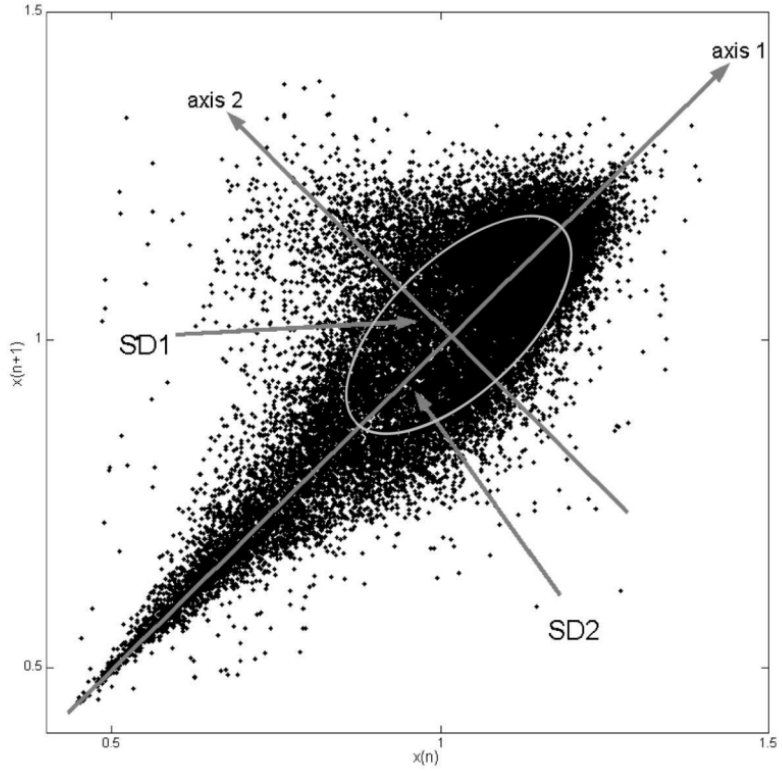

Figure 2.6: An ellipse fitted to the Poincaré plot with descriptors SD1 and SD2 [36].

Chapter 3

Windkessel model

3.1 Windkessel effect

The study of cardiovascular hemodynamics examines blood flow within the cardiovascular system. The interaction of blood pressure, resistance, and cardiac output determines hemodynamics. An important phenomenon in cardiovascular hemodynamics is the Windkessel effect. The phrase "Windkessel effect" is used in medicine to describe how the interaction of the stroke volume, the resistance of the smaller arteries and arterioles, and the compliance of the aorta and large elastic arteries (Windkessel vessels) shapes the waveform of arterial blood pressure. The term "windkessel" ("air chamber" in German) refers to a component of an antique fire engine that functions somewhat like the elastic aorta, which influences arterial pulses (Figure 3.1). German physiologist Otto Frank described an early Windkessel model in a paper that was published in 1899 [37]. All of the circuit is filled with water, with the exception of the chamber's air pocket. Pumped water into the chamber compresses the pocket's air and forces water back toward the pump as it exits the chamber. The air in the pocket is compressible, simulating the major artery's elasticity and extensibility when blood is pushed into it by the heart ventricle. Arterial compliance is the term often used to describe this effect. The resistance that water faces when it exits the Windkessel and returns to the pump mimics the resistance that blood experiences as it passes through the arterial tree, passing from main arteries to smaller arteries, arterioles, and capillaries, because of the vessel diameter diminishing. Peripheral resistance is the term used to describe this flow resistance. Given a constant ratio of air pressure to air volume in the chamber and a fluid flow through the pipes connecting the air chamber to the pump that is proportionate to fluid pressure according to Poiseuille's law, the water flow

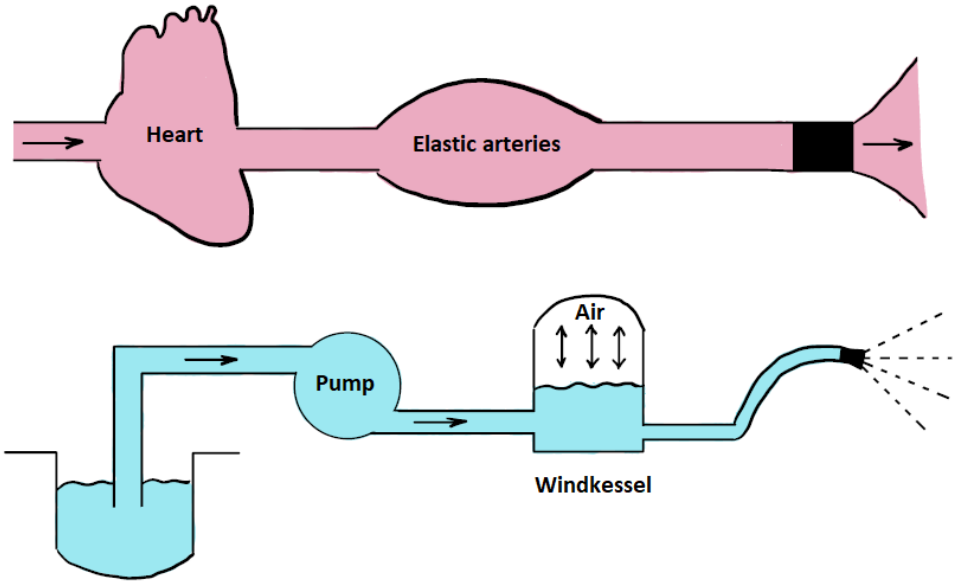

Figure 3.1: The analogy of Windkessel effect.

and pressure can be found by solving the following differential equation:

$$I(t) = \frac{P(t)}{R} + C\frac{dP(t)}{dt} \tag{3.1}$$

where C is the constant ratio of air pressure to air volume, R is the flow-pressure proportionality constant, I(t) is the water flow out of the pump as a function of time measured in volume per time units and P(t) is the water pressure as a function of time measured in force per area units. The relationship between the current, I(t), and the time-varying electrical potential, P(t), in the electrical circuit in Figure 3.2 is described by the same equation. This model is most often called the two-element Windkessel model since it only has two passive components: a resistor and a capacitor. Within the physiological system, I(t) represents the blood flow rate in cm^3/s from the heart to the aorta (or pulmonary artery); P(t) represents the blood pressure in mmHg within the aorta (or pulmonary artery); C represents the arterial compliance within the aorta (or pulmonary artery) in $cm^3/mmHg$ and R represents the peripheral resistance within the systemic (or pulmonary) arterial system in $mmHgs/cm^3$. I(t) = 0 during diastole, when there is no heartbeat, and P(t) may be precisely calculated using the Windkessel equation:

$$P(t) = P(t_d)e^{-(t-t_d)/RC} \tag{3.2}$$

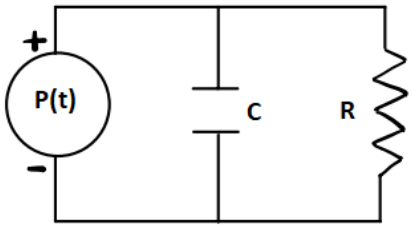

Figure 3.2: Two-element Windkessel model.

where P(t_d) is the blood pressure in the aorta (or pulmonary artery) at the beginning of diastole and t_d is the time at which diastole begins.

More intricate models with three or four factors have been suggested to better fit the data from the studies [38]. The Broemser model is an additional circulatory system model, also known as the three-element Windkessel model [39]. In order to represent blood flow resistance caused by the aortic or pulmonary valve, the Broemser model adds a resistive element between the pump and the air chamber to the two-element Windkessel model (Figure 3.3). For the three-element Windkessel model, the differential equation is as follows:

$$(1 + \frac{R_1}{R_2})I(t) + CR_1\frac{dI(t)}{dt} = \frac{P(t)}{R_2} + C\frac{dP(t)}{dt} \tag{3.3}$$

where R2 is the peripheral resistance and R1 is the resistance caused by the pulmonary or aortic valve. When I(t) and its derivatives with respect to time equal zero during diastole, the three-element Windkessel equation is solved as follows:

$$P(t) = P(t_d)e^{-(t-t_d)/(R_2C)} \tag{3.4}$$

If the inductor is added to the circuit with three elements, it becomes the four-element Windkessel model (Figure 3.4). In the hydrodynamic model, an inductor in the main branch of the circuit is stated to replicate the fluid's inertia, which was neglected in the two and three-element Windkessel model. The differential equation for this four-element Windkessel model becomes:

$$(1 + \frac{R_1}{R_2})I(t) + (R_1C + \frac{L}{R_2})\frac{dI(t)}{dt} + LC\frac{d^2I(t)}{dt^2} = \frac{P(t)}{R_2} + C\frac{dP(t)}{dt} \tag{3.5}$$

The exponentially declining pressure function with decay time constant R_2C that we obtain by solving for P(t) during diastole, when I(t) and its derivatives vanish, is identical to that of the three-element Windkessel model (3.4).

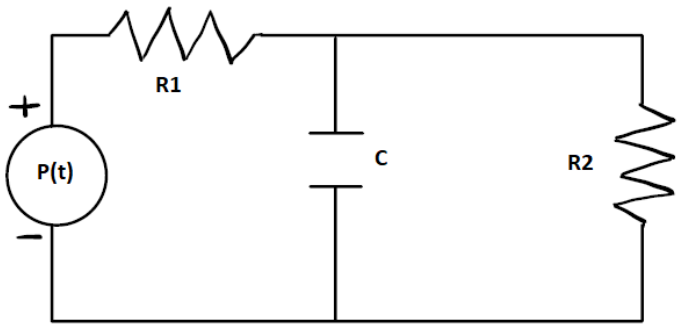

Figure 3.3: Three-element Windkessel model.

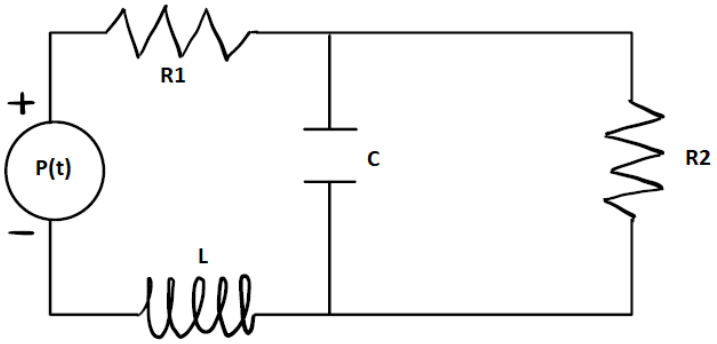

Figure 3.4: Four-element Windkessel model.

The relationship between blood pressure and blood flow in the arterial system is explained by the Windkessel model. The elastic portion of the Windkessel expands during systole (Figure 3.5A), when the heart beats and pumps blood into the arteries, storing energy and preserving a comparatively steady blood pressure. The elastic part of the Windkessel contracts during diastole (Figure 3.5B), when the heart slows down and blood still passes through the arteries, releasing energy and keeping blood pressure largely steady. The Windkessel model is also used to comprehend how the cardiovascular system is affected by aging and illness. The vascular system's elastic qualities may deteriorate with age, which can result in a loss of compliance and a rise in blood pressure. Studies employing nuclear magnetic resonance (NMR) methods on humans verified the age-related increase in elastic resistance [40]. Reduced elastin content and a relative rise in collagen content are the characteristics of age-related changes in arterial wall properties, which lead to

an increase in arterial stiffness. Less blood can be stored in the Windkessel and is therefore sent to the periphery when the core arteries are more rigid. Apart from arterial stiffness, the performance of the Windkessel function can also be influenced by arterial size and cardiac output. In average, women have smaller vessels than men do, which permits the Windkessel to store less systolic blood for later delivery during diastole [41]. Therefore, variations in these characteristics based on gender may be a factor in women's lower Windkessel function. Similar to age and gender factors, diseases like hypertension and atherosclerosis can also alter the arterial system's elastic characteristics, changing blood flow and pressure. Pathophysiologic problems can be attributed to the degeneration of the aorta's elastic qualities. These conditions include the accumulation of smooth muscle cells, calcium, and connective tissue or the presence of abnormal elastin [42].

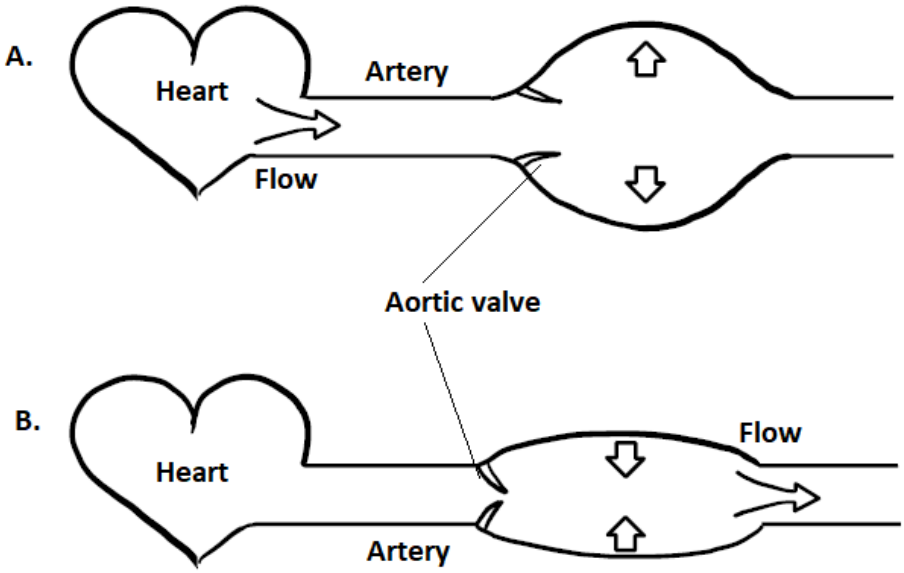

Figure 3.5: The concept of the Windkessel effect during ventricular systole (A) and diastole (B).

3.2 Hypertension in cancer patients

According to studies, the most frequent comorbidity seen in individuals with cancer is hypertension [43]. Research evaluating the correlation between high blood pressure and various forms of cancer exhibit inconsistencies [44]. The only cancer type that has been consistently linked to hypertension is renal cell carcinoma [45].

The study of Seretis et al. (2019) identified potential positive connections between hypertension and the risk of colorectal, breast, endometrial, liver, and oesophageal cancers in addition to confirming the known link between hypertension and the risk of kidney cancer [44]. Although the exact biological mechanisms causing this relationship are unknown, some theories include chronic renal hypoxia [46], lipid peroxidation [47] and deregulation of renin-angiotensin system [48].

The treatment of hypertension, rather than hypertension per se, may be associated with increased cancer risk. The increased prevalence of hypertension brought on by the use of angiogenesis inhibitors in targeted cancer therapy has led to a recent spike in interest in hypertension in patients with underlying malignancy [49]. From a cardiovascular point of view, the patient with a tumor who is receiving potentially toxic oncologic therapy has an increased risk of developing adverse cardiovascular events. This risk increases in the presence of concurrent arteriosclerosis (cronic or secondary to medication), especially if adequate compensation is not received. Drugs that interact with the VEGF (vascular endothelial growth factors) pathways are the most often implicated in the development of hypertension among the more recent cancer medications [50]. Anti-VEGF-induced hypertension is influenced by a number of variables, including the particular molecule employed, dosage, treatment plan, patient age, and the existence of cardiovascular risk factors. The inibition of VEGF receptors induces the suppression of nitric oxide synthesis which in turn promotes the vasoconstriction and therefore also the increase in flow resistance and blood pressure [51]. For this reason before starting VEGF inhibitor therapy, blood pressure should be adequately controlled. As VEGF inhibitor therapy progresses, antihypertensive medications should be titrated to achieve the appropriate blood pressure values.

The association between hypertension and malignancy might be confounded by other risk factors that are common in hypertensive patients, such as diabetes, obesity [52] , smoking [53], and alcohol consumption. Patients with type 2 diabetes or obesity are more likely to have an elevated risk of cancer progression due to the acceleration of oxidative stress within tumor cells caused by increasing levels of circulating or local reactive oxygen species (ROS) obtained from increased adipose tissue in the tumor environment.

Chapter 4

Computational models

4.1 Parameter sensitivity of solutions

One approach to analyze the HRV in cancer patients is through the use of nonlinear differential equations. Modeling HRV in cancer patients with nonlinear differential equations has the benefit of capturing the intricate, nonlinear dynamics of the ANS and cardiovascular system. This may lead to a more precise comprehension of the physiological mechanisms that underlie HRV in cancer patients. The effects of various interventions, such as cancer therapies, on HRV can also be simulated using nonlinear differential equations. This work explored the modelling of HRV using a particular nonlinear differential equation called Van der Pol equation.

The first step was the analysis of parameter sensitivity of the solutions. In other words, the goal was to determine how much the solutions change on the model parameters. Without any external forcing, in the Van der Pol equation:

$$\frac{d^2x}{dt^2} - \mu(1 - x^2)\frac{dx}{dt} + x = 0 \tag{4.1}$$

x represents the displacement, t is time, and μ is a parameter controlling the nonlinearity and damping.

The sensitivity of solutions of the Van der Pol oscillator to its parameters, particularly μ, can be quite significant. The parameter μ determines the strength of the damping in the system. Higher values of μ lead to stronger damping, while lower values lead to weaker damping. As a result, changes in μ can significantly alter the behavior of the oscillator. For instance, with low μ, the oscillator may exhibit sustained oscillations or chaotic behavior, while with high μ , it may approach a stable equilibrium quickly. The term $\mu(1 - x^2)\frac{dx}{dt}$ represents nonlinear damping. This term is responsible for the transition between stable and oscillatory behavior. Changes in μ can thus impact the strength of this nonlinear effect, leading to changes in the amplitude and frequency of oscillations. When μ is large, the

damping force dominates, causing the oscillations to decay rapidly. As a result, the system approaches its equilibrium state quickly without exhibiting significant oscillatory behavior. The solutions of the oscillator become more akin to simple exponential decay towards the equilibrium point. In contrast, when μ is small, the damping force is weak. The oscillator exhibits sustained oscillations, and the amplitude of oscillations may remain relatively constant or slowly decrease over time. The system's behavior is characterized by a balance between the nonlinear restoring force and the weak damping.

Furthermore, initial conditions are essential for obtaining a unique solution to the differential equation. To solve the equation (4.1), you need to know the values of $x(t = t_0) = x_0$ that determines the starting position of the oscillator and of $\frac{dx}{dt}(t = t_0) = v_0$ that specifies the initial velocity of the oscillator at time t_0. Depending on the specific values of x_0 and v_0 , the behavior of the Van der Pol oscillator may exhibit various phenomena such as sustained oscillations, relaxation oscillations, or chaotic behavior. Sustained oscillations refer to the persistent, repetitive motion exhibited by a dynamic system without decay or growth in amplitude over time. Relaxation oscillations occur when the system alternates between fast, transient periods of rapid change and slower, more gradual relaxation towards a stable equilibrium. Chaotic behavior refers to the unpredictable, aperiodic motion exhibited by the system under certain conditions.

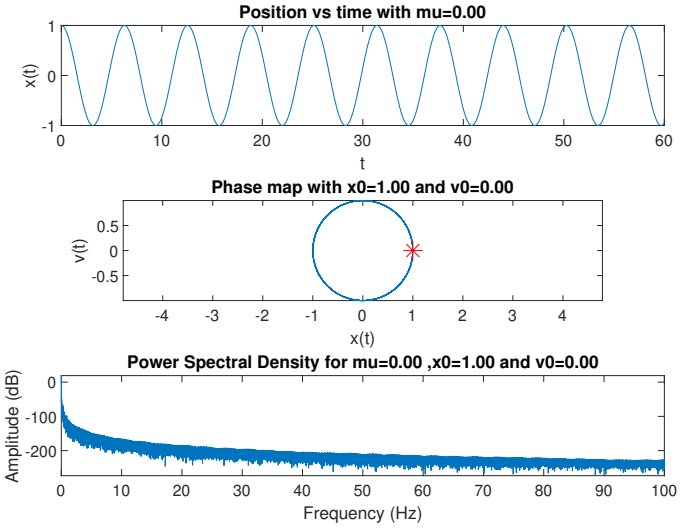

Figure 4.1: Time series of the VdP oscillator, phase map and power spectral density plot with parameter μ=0.

ODE45 function was used to solve ordinary differential equations numerically

(Appendix A Listing A.1). To solve the VdP equation and use ODE45 function, the second order ODE must be converted into two first order ODEs:

$$\begin{cases} x_1 = x(t) \\ x_2 = x'(t) \end{cases} \tag{4.2}$$

Differentiating the system of two equations (4.2) we obtain:

$$\begin{cases} x_1' = x_2 \\ x_2' = \mu(1 - x_1^2)x_2 - x_1 \end{cases} \tag{4.3}$$

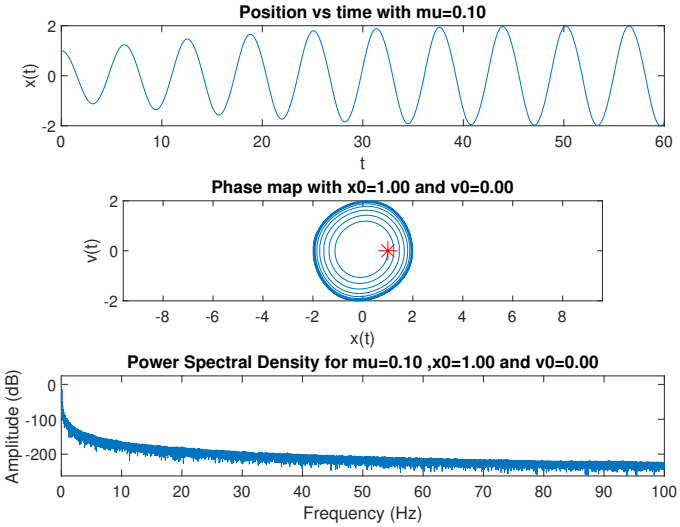

Figure 4.2: Time series of the VdP oscillator, phase map and power spectral density plot with parameter μ=0.1.

To analyze the parameters sensitivity of solution, the initial conditions of the system (4.3) remained constant $x_1(0) = x(0) = 1$ and $x_2(0) = x'(0) = 0$. Different numerical values have been applied to the parameter μ. Time series of the VdP oscillator, phase maps and power spectral density plots were represented to inspect the parameters sensitivity of solution. To generate a phase portrait (also known as a phase plane or phase diagram) for the Van der Pol oscillator, the trajectory of the system was plotted in the phase space defined by the displacement x and its derivative $\frac{dx}{dt}$. Phase map is a graphical representation of the behavior of a dynamical system in a multi-dimensional state space. The Power Spectral Density (PSD) of the Van der Pol oscillator describes how the power of the signal generated by the oscillator is distributed across different frequencies. PWELCH function and

the sampling frequency equal to 200 Hz were used to plot the PSD. The maximum frequency of the components of interest in the ECG is generally less than 100 Hz. To avoid aliasing, the sampling rate must be at least double the maximum. For this reason the sampling frequency was chosen to be 200 Hz. The equation (4.1) becomes the standard equation for a harmonic oscillator when $\mu = 0$ (on the top of Figure 4.1):

$$y'' + y = 0 \tag{4.4}$$

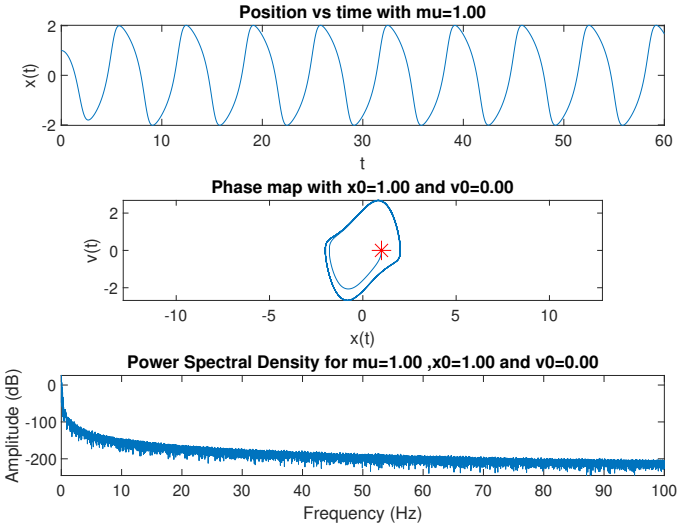

Figure 4.3: Time series of the VdP oscillator, phase map and power spectral density plot with parameter μ=1.

In this case the oscillator exhibits the circumference in phase map (in the middle of Figure 4.1). Situations with values of the μ parameter equal to 0.1 (Figure 4.2), 1 (Figure 4.3) and 3 were examined (Figure 4.4).

In the time series plots when μ value increases, the frequency of oscillation decreases. Also the shape of the oscillations in the phase space can vary widely depending on the value of μ. In case of small nonlinearity ($0<\mu \ll 1$), the shape may resemble nearly circular orbits. As μ increases, the shape can become more complex and show variations in amplitude and the solutions tend to approach the limit cycle in a shorter and shorter time interval.

A slightly modified version of VdP equation expressed by equation (2.8), gives a better model of the cardiac activity. In this equation (2.8 α is the factor that changes the pulse shape of a heartbeat in response to a stimulus, and x is the length of a heart fiber. The parameters ν_1 and ν_2 combine to form an asymmetric term that modifies the damping term included in the classic VdP equation; e stands

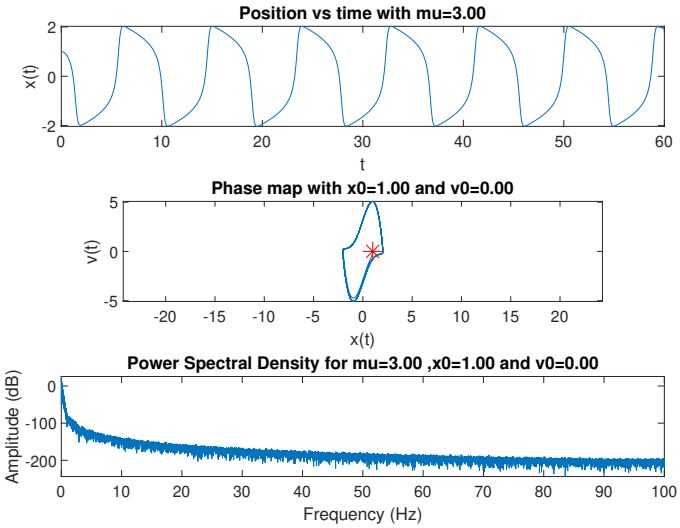

Figure 4.4: Time series of the VdP oscillator, phase map and power spectral density plot with parameter μ=3.

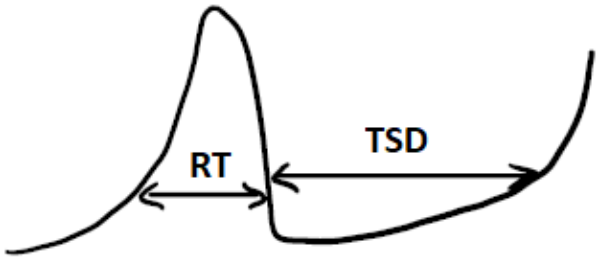

Figure 4.5: Representation of refraction time (RT) followed by time of spontaneous depolarization (TSD).

for ventricular contraction period; and d is a factor that emerges when a cubic term is substituted for the harmonic forcing in the classic VdP equation [29]. The parameters v_1 and v_2 directly affect the diastolic period and the resting potential of the pacemaker, the parameter α directly affects the amplitude of the output and the value of e and d affect the depolarization time of the pacemaker [54].

A variation in parameter α causes changes in the diastolic and refractory periods [54]. During the refractive phase the cell is immune to external excitation when

the action potential is generated. After the refractory period, the spontaneous depolarization (diastolic period) starts (Figure 4.5).

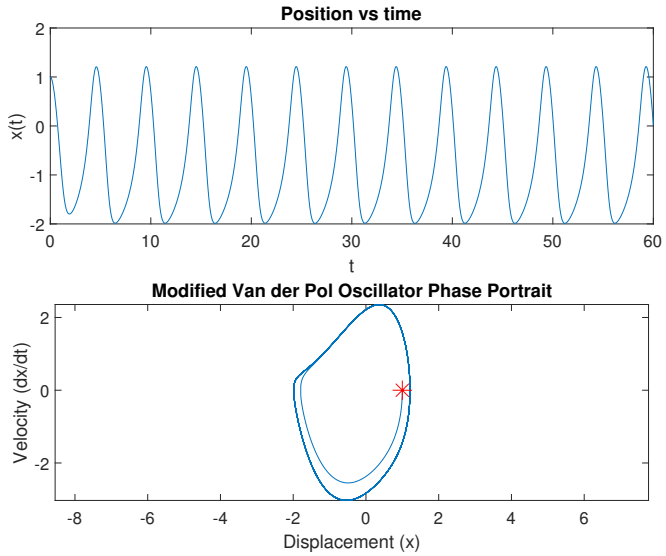

Figure 4.6: Time series and phase maps of modified VdP oscillator with α=1, ν_1=0.83, ν_2=-0.83, d=3 and e=6.

By incorporating system parameters α, ν_1, ν_2, d and e into the conventional VdP oscillator, it becomes possible to alter the actuation potential's firing frequency without altering the duration of the refractory period [54]. In this case the two first order ODEs are:

$$\begin{cases} x_1' = x_2 \\ x_2' = -\alpha x_2(x_1 - \nu_1)(x_1 - \nu_2) + x_1(x_1 + d)(x_1 + e) \end{cases} \tag{4.5}$$

with constraints that ν_1 and ν_2 must have the opposite signs to preserve the self-oscillatory character of the system and α, d and e must be positive [54].

The values of initial conditions were held constant: x(0)=1 and v(0)=0. The values of system parameters were proposed by Grudzinski et al. (2004): α=1, ν_1=0.83, ν_2=-0.83, d=3 and e=6 [54]. The solutions with these parameters were plotted in Figure 4.6. It is possible to see that unlike the previous case with conventional VdP oscillator, the time series and phase maps present the differences with modified VdP equation, especially in phase maps. The phase maps became asymmetric thanks to the introduction of parameters ν_1 and ν_2 which represent an asymmetric damping term related to the voltage in the VdP equations. As the value of α increases, keeping the values of other parameters constant (ν_1=0.83, ν_2=-0.83, d=3 and e=6), it's possible to note the changes in the pulse form and

the transition from less frequent to more frequent oscillations (Figures 4.7-4.9). Also the phase portrait presents some changes. When α value increases, the limit cycle becomes narrower, it could indicate that the oscillations of the system are occurring with a small amplitude.

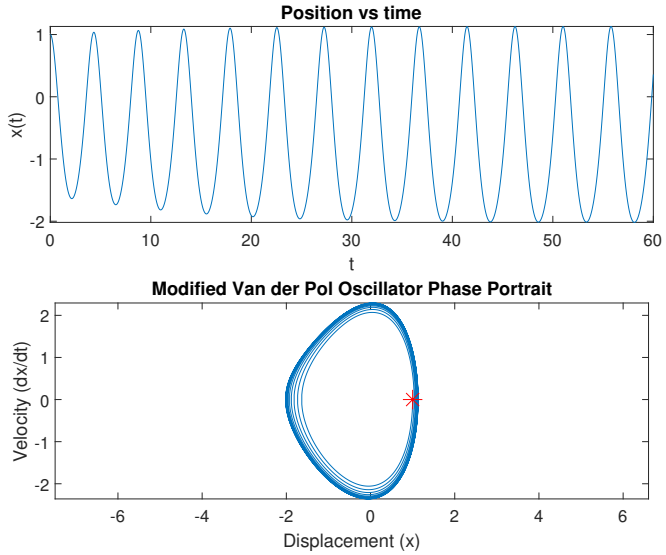

Figure 4.7: Time series and phase maps of modified VdP oscillator with α=0.1, ν_1=0.83, ν_2=-0.83, d=3 and e=6.

The variations of ν_1 and ν_2 values, keepin other parameters constant (α=1, d=3 and e=6.), bring to drastic changes in the waveform and in phase portrait (Figure 4.10-4.12). It is noted that for low values of ν_1 and ν_2, the oscillations decrease in amplitude and the phase map representation is far from the limit circle.

If we increase the value of d parameter, the oscillations frequency increases too and the shape of limit cycle becomes more narrow (Figures 4.13-4.15).

If the values of e are changed, from the plots obtained one can note that as the value increases, keeping other parameters constant (α=1, ν_1=0.83, ν_2=-0.83, d=3), the frequency of the oscillation increases, meanwhile the phase map plot seems to remain invariable (Figures 4.16-4.18).

In the work of Lopez-Chamorro et al. (2018) the optimal modified VdP parameters for heartbeats samples were obtained through use of Genetic Algorithm (GA) throughout the Dynamic Time Warping alignment method (DTW) [55] (Table 4.1).

All these values were considered for analyzing the sensitivity of solutions to parameters (Appendix A Listing A.2). The graphs of time series, the phase maps and the graphs of power spectral density were plotted. There were no differences between the graphs using the optimal values perceptible to the human eye. So to

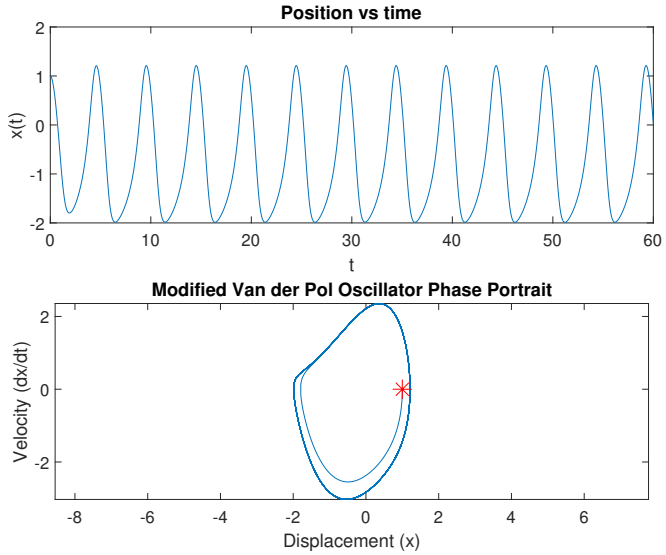

Figure 4.8: Time series and phase maps of modified VdP oscillator with α=1,ν_1=0.83, ν_2=-0.83, d=3 and e=6.

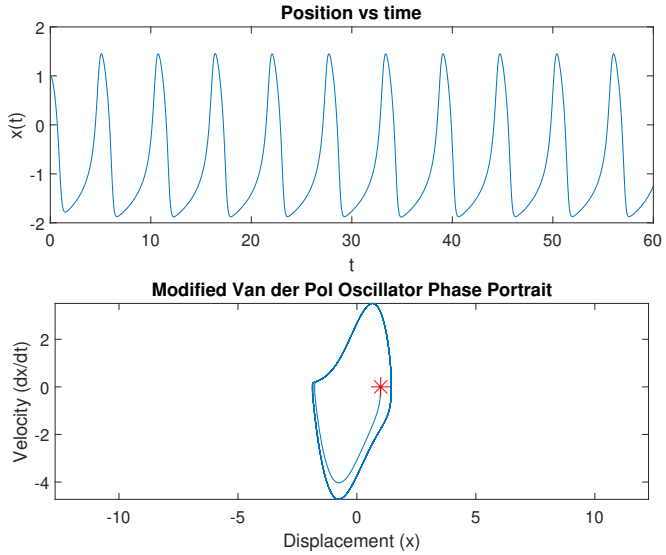

Figure 4.9: Time series and phase maps of modified VdP oscillator with α=3, ν_1=0.83, ν_2=-0.83, d=3 and e=6.

see the key points of plots, therefore it is enough to to analyze the graphs with the optimal values of the first row of the Table 4.1 (Figure 4.19). From the Figure

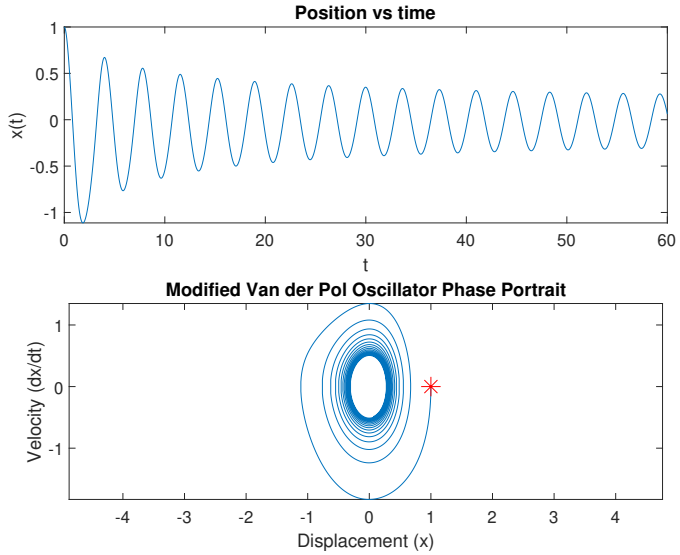

Figure 4.10: Time series and phase maps of modified VdP oscillator with ν_1=0.1 and ν_2=-0.1, α=1, d=3 and e=6.

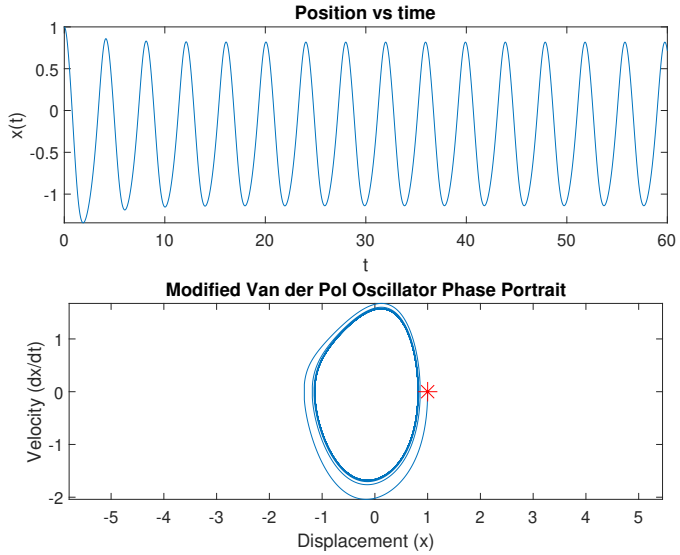

Figure 4.11: Time series and phase maps of modified VdP oscillator with ν_1=0.5 and ν_2=-0.5, α=1, d=3 and e=6.

4.19 it's possible to see how the time series resembles action potentials captured from a cardiac pacemaker's real cells [54] (Figure 4.28) more than in the previous

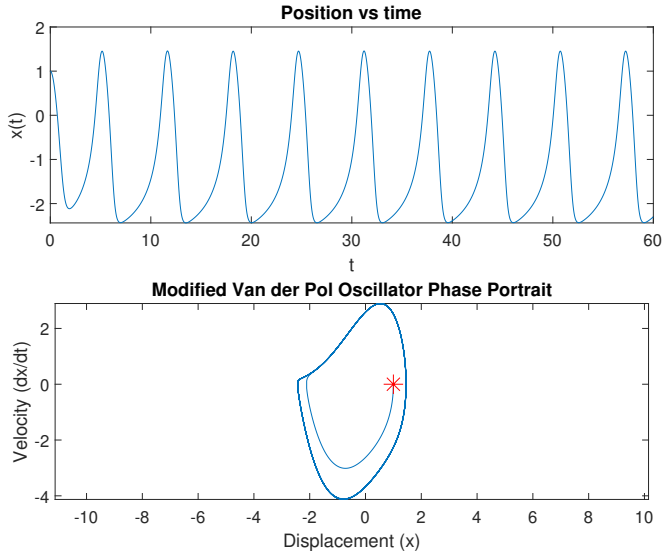

Figure 4.12: Time series and phase maps of modified VdP oscillator with ν_1=1 and ν_2=-1, α=1, d=3 and e=6.

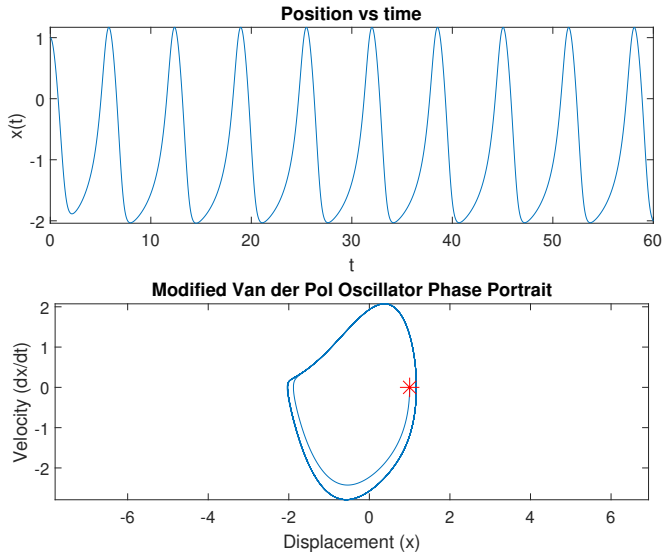

Figure 4.13: Time series and phase maps of modified VdP oscillator with d=2.5, α=1, ν_1=0.83, ν_2=-0.83, e=6.

cases (Figures 4.1-4.4 and 4.6-4.18). The limit cycle appears narrow in the phase portrait, this may be due to the increase of the nonlinearity term $\frac{x(x+d)(x+e)}{ed}$. Also

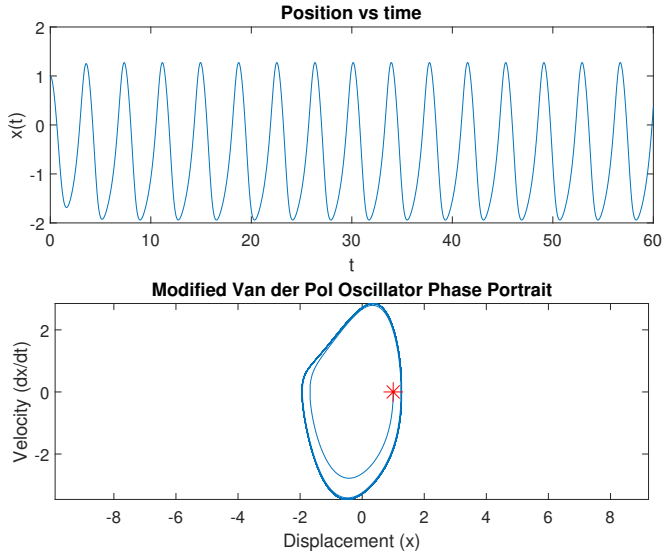

Figure 4.14: Time series and phase maps of modified VdP oscillator with d=4, α=1, ν_1=0.83, ν_2=-0.83, e=6.

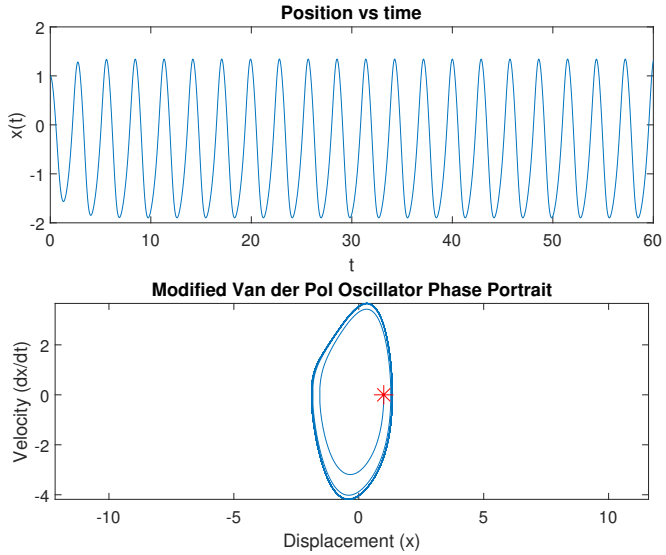

Figure 4.15: Time series and phase maps of modified VdP oscillator with d=6, α=1, ν_1=0.83, ν_2=-0.83, e=6.

in this case with new parameter values, it is important to analyze the solution sensitivity. Subsequently the time series graphs and phase maps are represented

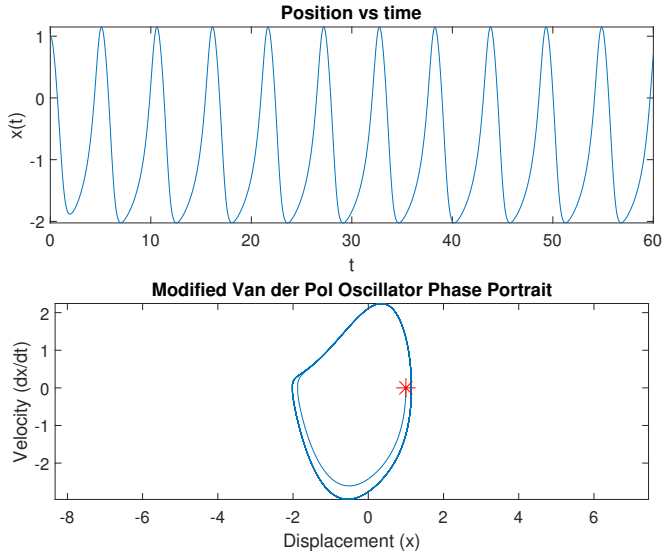

Figure 4.16: Time series and phase maps of modified VdP oscillator with e=4, α=1, ν_1=0.83, ν_2=-0.83, d=3.

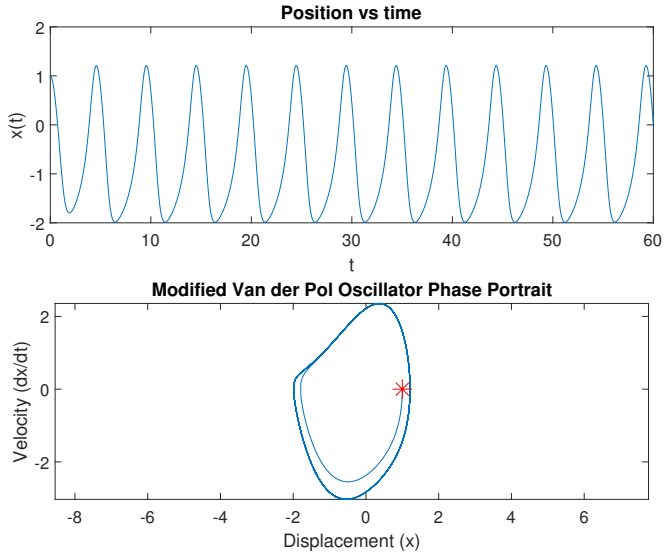

Figure 4.17: Time series and phase maps of modified VdP oscillator with e=6, α=1, ν_1=0.83, ν_2=-0.83, d=3.

for different values of parameters α, ν_1, ν_2, d and e close to the values of Table 4.1 (Figures 4.20 - 4.27).

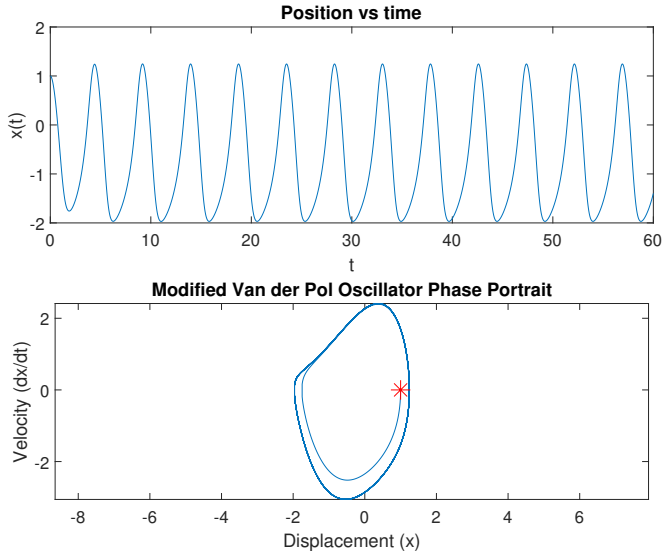

Figure 4.18: Time series and phase maps of modified VdP oscillator with e=8, α=1, ν_1=0.83, ν_2=-0.83, d=3.

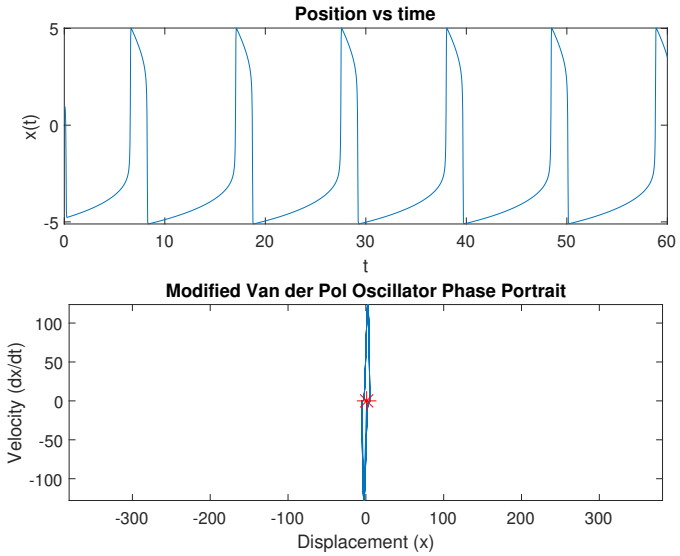

Figure 4.19: Time series of the modified VdP oscillator and phase map with parameters α=5.598, ν_1=2.5151, ν_2=-2.5151, d=10.6335 and e=10.0548.

Then the forcing factor $Asin(\omega t)$ was added in modified VdP equation (2.8).

Table 4.1: Optimal modified VdP system parameters.

α	ν_1	ν_2	d	e
5.5982	2.5151	−2.5151	10.6335	10.0548
7.0488	2.1632	−2.1632	14.1948	7.87016
14.6852	2.8377	−2.8377	13.1039	8.27039
14.9178	2.8719	−2.8719	8.26114	13.6683

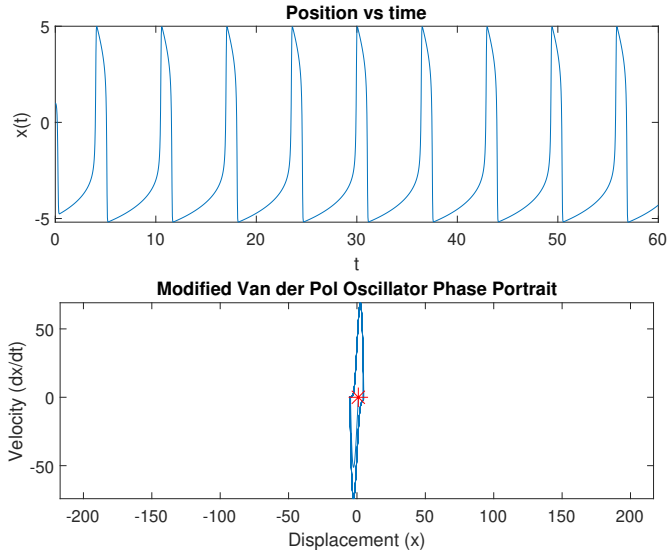

Figure 4.20: Time series of the modified VdP oscillator and phase map with parameters α=3, ν_1=2.5151, ν_2=-2.5151, d=10.6335 and e=10.0548.

The equation with modified VdP oscillator and forcing term becomes:

$$\ddot{x} + \alpha(x - \nu_1)(x - \nu_2)\dot{x} + \frac{x(x+d)(x+e)}{ed} = Asin(\omega t) \tag{4.6}$$

where, A represents the amplitude of the sinusoidal forcing term, and ω represents the pulsation of the forcing term. The values of these parameters were proposed by Raja et al. 2017) using feedforward artificial neural networks (FF-ANNs) optimized with genetic algorithms hybrid through interiorpoint algorithm (IPA) [29]: A=2.5 and ω=1.9 (Appendix A Listing A.3). The sinusoidal forcing term introduces an external periodic influence into the system, which can model various phenomena such as external stimuli in biological systems. Figure 4.29 shows the response of the oscillator for α=1, ν_1=0.83, ν_2=-0.83, d=3, e=6 A=2.5 and ω=1.9.

If we change the value of ω,keeping the same values of other parameters, we

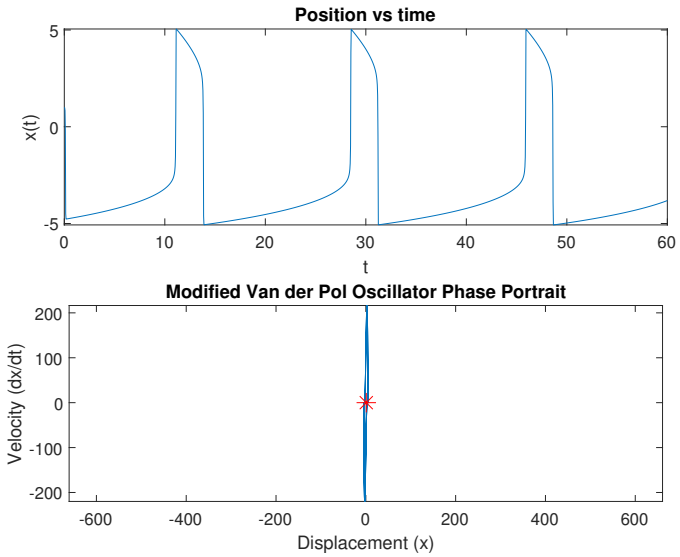

Figure 4.21: Time series of the modified VdP oscillator and phase map with parameters α=10, ν_1=2.5151, ν_2=-2.5151, d=10.6335 and e=10.0548.

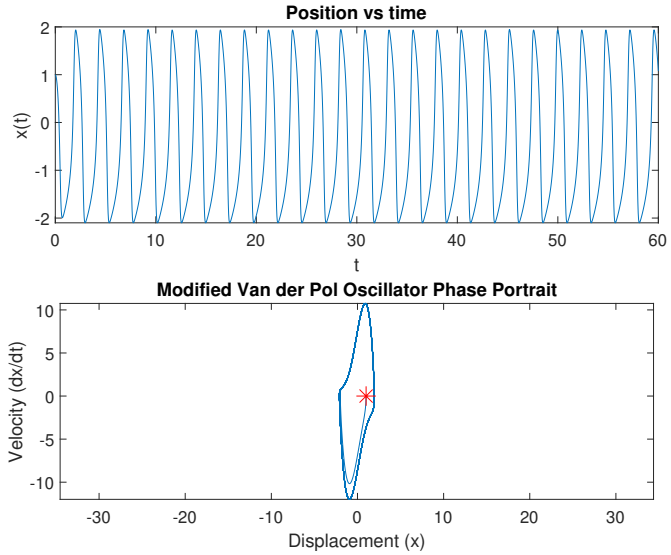

Figure 4.22: Time series of the modified VdP oscillator and phase map with parameters α=5.598, ν_1=1, ν_2=-1, d=10.6335 and e=10.0548.

can note that greater values of ω will smooth the wave shape, while smaller values will distort the output (Figures 4.30 and 4.31). Greater values of ω increase the

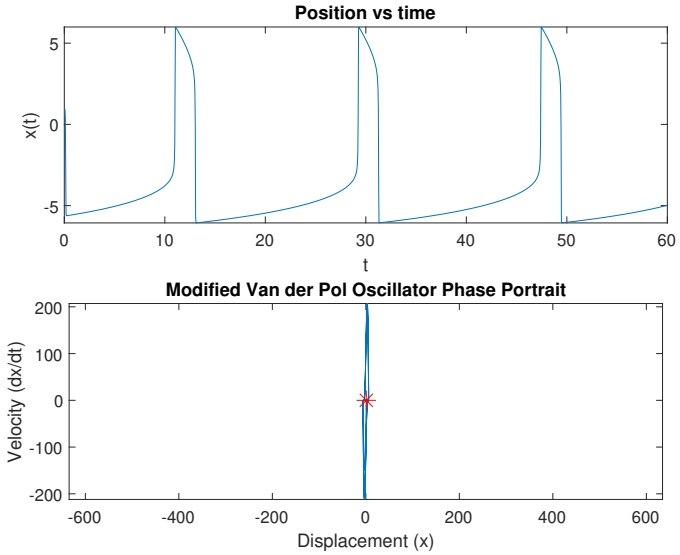

Figure 4.23: Time series of the modified VdP oscillator and phase map with parameters α=5.598, ν_1=3, ν_2=-3, d=10.6335 and e=10.0548.

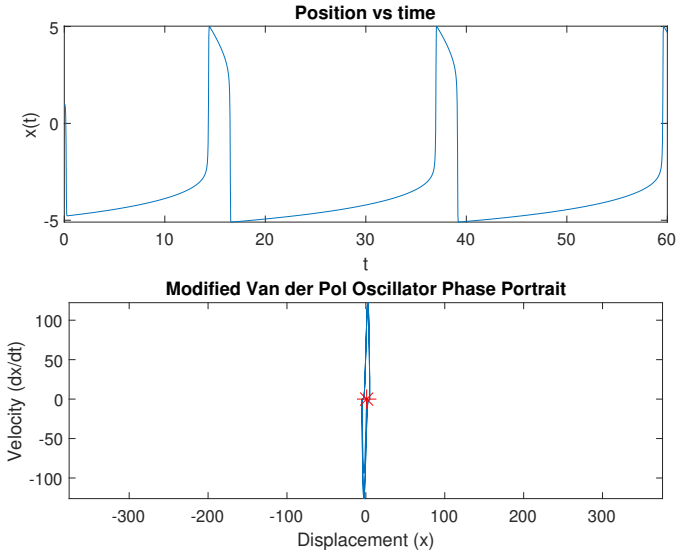

Figure 4.24: Time series of the modified VdP oscillator and phase map with parameters α=5.598, ν_1=2.5151, ν_2=-2.5151, d=7 and e=10.0548.

oscillation frequency making waves more regular from the point of view of shape.

If the value of amplitude of the sinusoidal forcing term changes drastically the

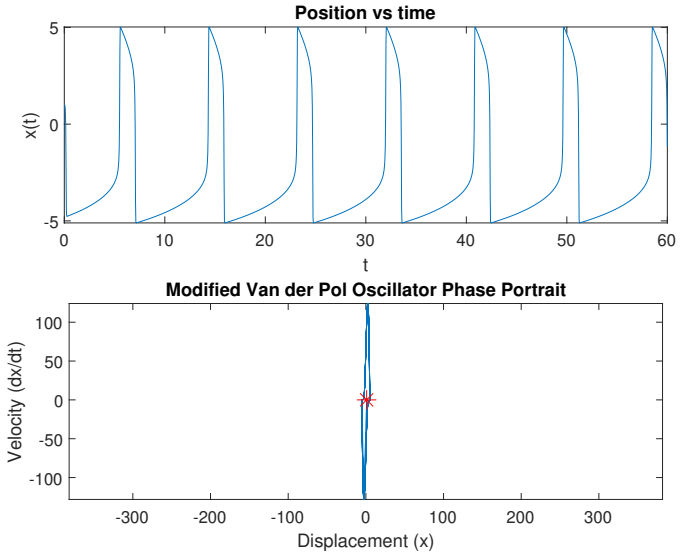

Figure 4.25: Time series of the modified VdP oscillator and phase map with parameters α=5.598, ν_1=2.5151, ν_2=-2.5151, d=12 and e=10.0548.

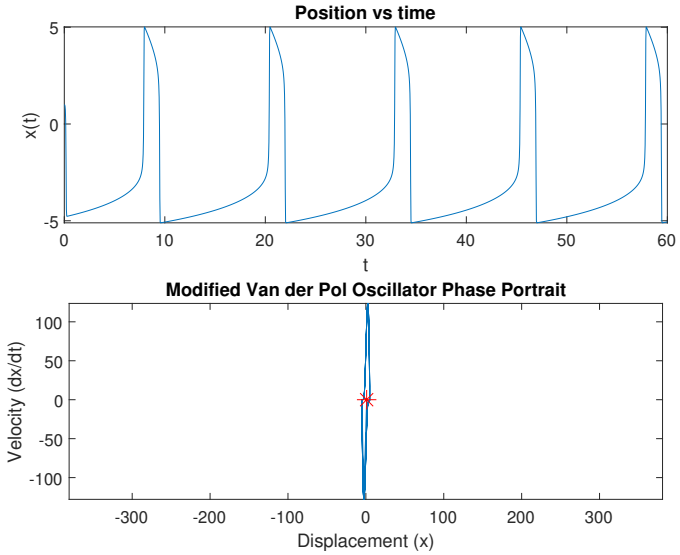

Figure 4.26: Time series of the modified VdP oscillator and phase map with parameters α=5.598, ν_1=2.5151, ν_2=-2.5151, d=10.6335 and e=8.

waves shape. Particularly, when A value increases, the waves become more irregular in shape.

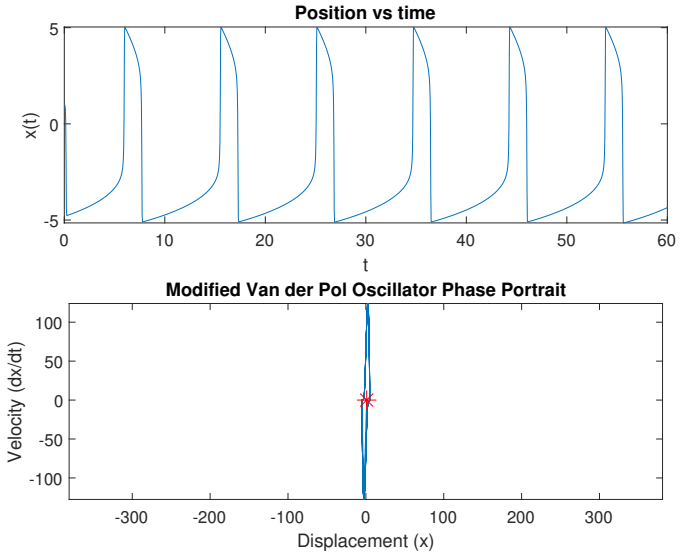

Figure 4.27: Time series of the modified VdP oscillator and phase map with parameters α=5.598, ν_1=2.5151, ν_2=-2.5151, d=10.6335 and e=12.

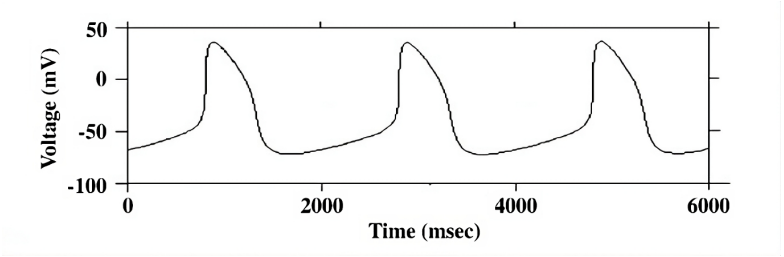

Figure 4.28: Action potentials recorded from the real cells of a cardiac pacemaker.

However, when the electromagnetic field is applied, the forcing term is simply not the same as $Asin(\omega t)$ but it gets a little complicated. The original RLC circuit is shown in Figure 4.34.

This circuit is described by the differential equation:

$$RI + L\frac{dI}{dt} + \frac{Q}{C} = V_{ext}(t) \tag{4.7}$$

wich can be differentiated respect to time to obtain a damped-driver harmonic oscillator equation:

$$L\frac{d^2I}{dt^2} + R\frac{dI}{dt} + \frac{1}{C}I = \frac{dV_{ext}}{dt} \tag{4.8}$$

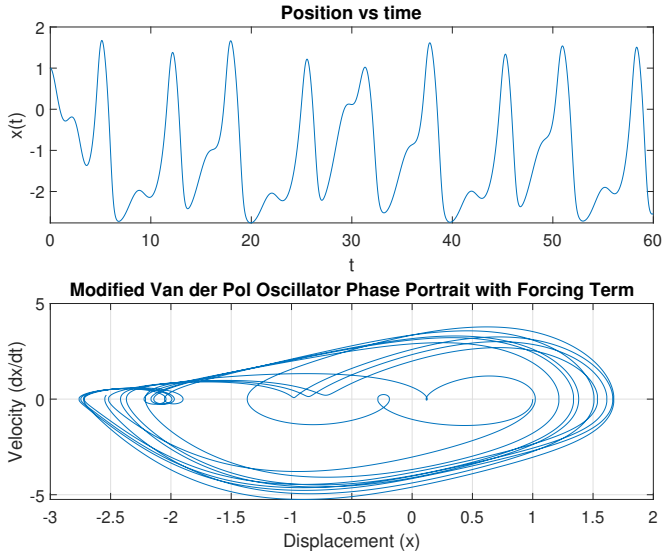

Figure 4.29: Time series of the modified VdP oscillator and phase map with amplitude A=2.5, pulsation ω=1.9 and parameters α=5.598, ν_1=2.5151, ν_2=-2.5151, d=10.6335 and e=10.0548.

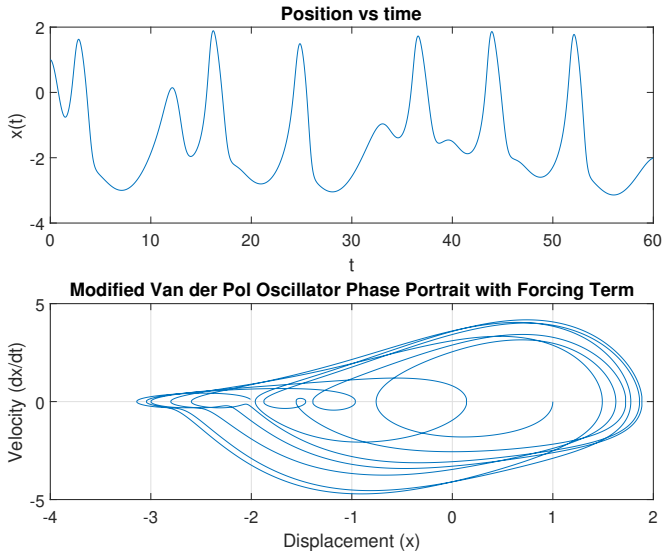

Figure 4.30: Time series of the modified VdP oscillator and phase map with amplitude A=2.5, pulsation ω=0.9 and parameters α=5.598, ν_1=2.5151, ν_2=-2.5151, d=10.6335 and e=10.0548.

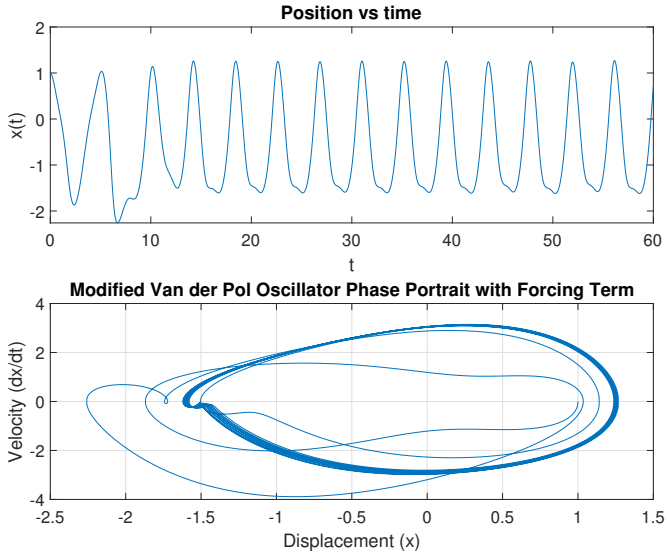

Figure 4.31: Time series of the modified VdP oscillator and phase map with amplitude A=2.5, pulsation ω=3 and parameters α=5.598, ν_1=2.5151, ν_2=-2.5151, d=10.6335 and e=10.0548.

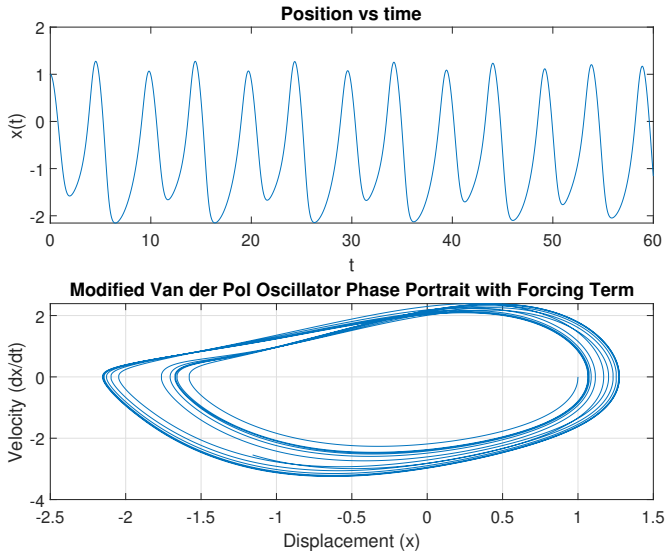

Figure 4.32: Time series of the modified VdP oscillator and phase map with amplitude A=0.5, pulsation ω=1.9 and parameters α=5.598, ν_1=2.5151, ν_2=-2.5151, d=10.6335 and e=10.0548.

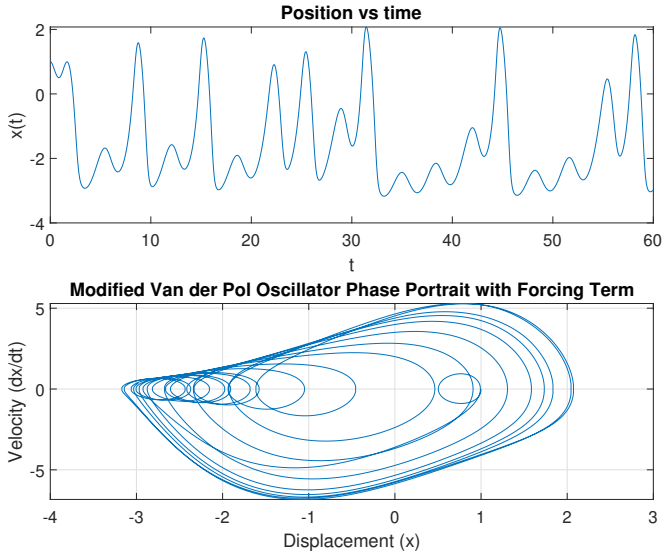

Figure 4.33: Time series of the modified VdP oscillator and phase map with amplitude A=5, pulsation ω=1.9 and parameters α=5.598, ν_1=2.5151, ν_2=-2.5151, d=10.6335 and e=10.0548.

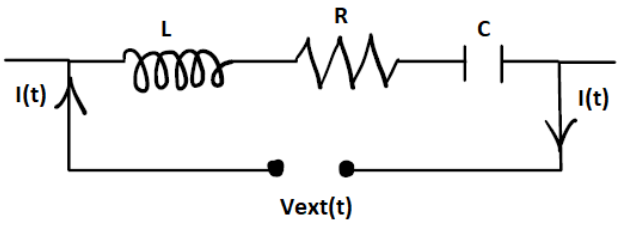

Figure 4.34: LRC circuit.

Since $I = \frac{dQ}{dt}$, the equation can be simplified:

$$\frac{d^2I}{dt^2} + (\frac{R}{L})\frac{dI}{dt} + \frac{1}{LC}I = (\frac{1}{L})\frac{dV_{ext}}{dt} \tag{4.9}$$

What Van der Pol did was to assume that the effective resistance in the circuit changes with the current according to $R = 3I^2 - \alpha$. In this mode, the VdP equation was obtained:

$$I'' + \frac{3I'}{L}(I^2 - \frac{\alpha}{3}) + \frac{I}{LC} = f(t) \tag{4.10}$$

where $f(t) = (\frac{1}{L})\frac{dV_{ext}}{dt}$. The modified VdP equation was specifically developed for hemodynamics and further assumed that the capacitive term of the equation was a

cubic nonlinear function of the current:

$$I'' + \alpha(I - \nu_1)(I - \nu_2)I' + \frac{I(I + d)(I + e)}{de} = f(t) \tag{4.11}$$

where $\alpha = \frac{3}{L}$. In case of applied electromagnetic fields

$$V_{ext} = V_0 sin(\omega t)[1 + asin(ft)] \tag{4.12}$$

,so

$$f(t) = f\frac{1}{L}\frac{dV_{ext}}{dt} = (\frac{V_0}{L})\omega cos(\omega t)[1 + asin(ft)] + afsin(\omega t)cos(ft) \tag{4.13}$$

However, the second term is much smaller than the first. Therefore, the forcing term can be simplified: $f(t) \approx \frac{V_0}{L}\omega cos(\omega t)[1 + asin(ft)]$. Also because $\omega \gg f$, it is possible to replace the term $cos(\omega t)$ with $sin(\omega t)$:

$$f(t) \approx (\frac{V_0}{L}\omega)sin(\omega t)[1 + sin(ft)] \tag{4.14}$$

So the final equation becomes:

$$I'' + \alpha(I - \nu_1)(I - \nu_2)I' + \frac{I(I + d)(I + e)}{de} = Asin(\omega t)[1 + sin(ft)] \tag{4.15}$$

where $A = \frac{V_0\omega}{L}$. The goal is to determine A value. We know that $V_0 = I_0R$, $I_0 = j_0A_0$ and $j_0 = \sigma E_0$ where j_0 is current density, A_0 is a cross-sectional area of the heart σ is heart conductivity and E_0 is amplitude of the electromagnetic signal. To determine the A value, it is necessary to know the $\frac{R}{L}$ value in the equation:

$$A = \frac{V_0\omega}{L} = \frac{R}{L}A_0\sigma E_0\omega \tag{4.16}$$

where ω is a carrier wave frequency ($\omega = 27.12MHz * 2\pi$) and f is tumor specific envelope frequency with values from 10 Hz to 150 kHz ($f = 10Hz * 2\pi$). The conductivity of myocardium is $\sigma \approx 0.16S/m$. For commercial pacemaker the resistance is on the order of $R = 1000\Omega$, the current is typically $I_0 = 10\mu A$, so from Ohm's law the voltage experienced by the heart is:

$$V_0 = I_0R = 10mV \tag{4.17}$$

The average cross-sectional area of the human heart is approximately 12-20 square centimeters. It is possible to estimate the value of current density from the formula with $S = 10cm^2$:

$$j_0 = I_0/S = \sigma E_0 \tag{4.18}$$

Knowing the values of j_0 and σ, it is possible to obtain the E_0 value:

$$E_0 = \frac{I_0}{S\sigma} = 6.25V/m \tag{4.19}$$

The medical device AUTEM produces electric field more or less equal to 3.8 V/m, this value is lower than of the pacemaker but of the same order of magnitude. It is important to underline that the value of E_0 obtained is much less than the value of $E_{max} = \frac{I_{max}}{\sigma A_0} = 25V/m$ where I_max is the value of current (50 mA) that can lead to cardiac arrest. The last term to determinate remains $\frac{R}{L}$. It is known that $\frac{R}{L} = \frac{1}{\tau}$ where τ is a time constant. Time constant can be approximated to diastolic phase time, parameter used to characterize the rate at which the ventricular pressure decreases during diastole. Typical values for the diastolic time constant in healthy individuals range from about 0.2 to 0.4 seconds. For parameters α, ν_1, ν_2, d and e the averages from Table 4.1 were taken as values: α=10.5625, ν_1=2.596975, ν_2=-2.596975, d=11.548335 and e=9.9659125. The script with these values and forcing term described previously was run on MATLAB (Appendix A Listing A.4) and the plots of time series and phase map were obtained (Figure 4.35).

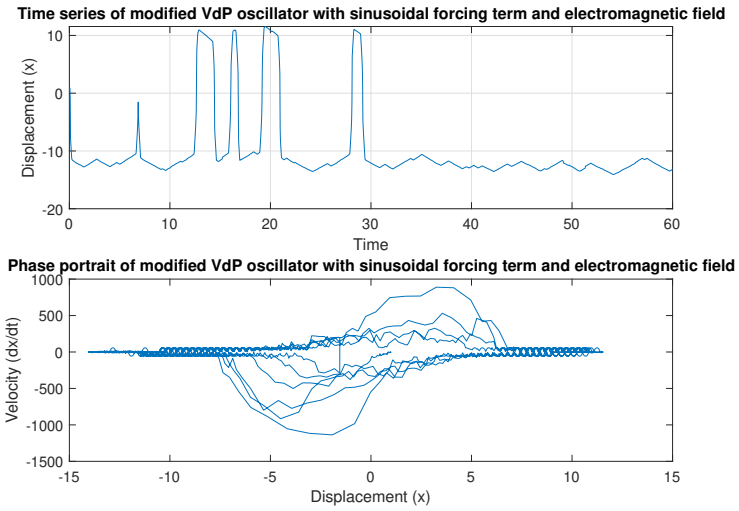

Figure 4.35: Time series of the modified VdP oscillator and phase map with carrier wave frequency ω= 27.12 MHz, tumor specific envelope frequency f=100 Hz and parameters α=5.598, ν_1=2.5151, ν_2=-2.5151, d=10.6335 and e=10.0548.

4.2 Database analysis

The patient database was provided by the Hospital Sirio Libanes (São Paulo, Brazil), especially by medical oncologist Frederico Perego Costa. The file Excel with two worksheets (ECG1 and ECG2), each of which has 988 columns and 8001 lines, was given. The first column was the time period in seconds and all other columns were the measure of voltage in millivolt and of pressure in mmHg due to the application of external electromagnetic fields in hertz. Here is the database scheme: ECG1 and ECG2 contained patient data subjected to electrical potential

Table 4.2: Patient data.

Time(s)	1(Hz)	1(Hz)	1(Hz)	2(Hz)	...	330(Hz)
0	0.4754	-0.0154	104.1749	0.3862	...	24.995
0.007	0.4753	-0.2646	104.0901	0.3846	...	24.995
...	...	...	...	...	...	...
55.993	-0.0419	-0.0119	101.2125	0.1586	...	24.995

measurement through different placements of the electrodes. All ECG signals were preprocessed. The waves were detrended to correct the baseline due to patient movement. Every applied frequency of electromagnetic field had three columns. The first one was ECG signal, the second column was the ECG gradient and last one was blood pressure measurement. ECG gradient involves measuring how rapidly the ECG signal changes over time. This might be useful for assessing the dynamics of the cardiac cycle, such as heart rate variability or the rate of change of specific features like the QRS complex. The measurement of systolic blood pressure (SBP) involves assessing the pressure in the arteries when the heart beats or contracts, pushing blood out into the body. The systolic blood pressure measurement is essential for assessing cardiovascular health and is a key indicator of heart function and vascular health. It's influenced by factors such as cardiac output, peripheral vascular resistance, and the elasticity of the arteries.

The goal was to obtain time series plots, phase maps and recursive maps from these data. Phase plots indicate the system behavior. Closed trajectory could suggest periodic behavior or a stable limit cycle. Recursive maps are represented as the voltage at each time step as a function of the voltage at the previous time step. In these plots the limit cycles characterize the system's oscillatory dynamics and could correspond to the sequence of electrical events in the heart cardiac cycle. The system tends to return to the same set of values, forming a closed trajectory.

To plot the time series, the script on MATLAB was run (Appendix A Listing A.5). The first thing to do when the script is run, is to insert two frequency value from 1 Hz to 330 Hz. The values must be integer numbers. To align two ECG

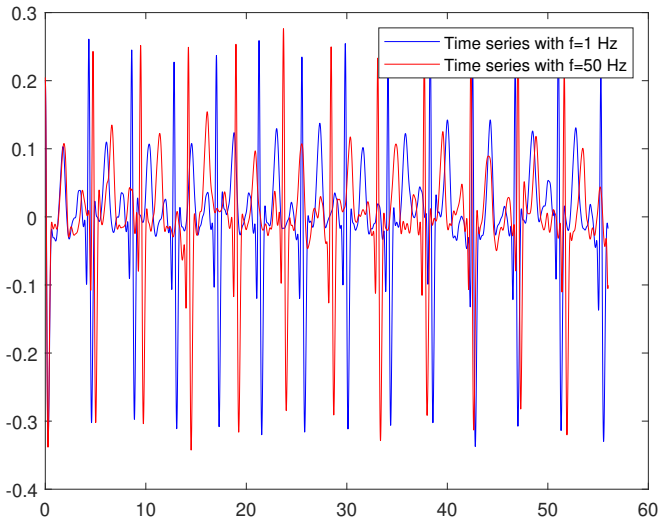

Figure 4.36: Time series obtained from data of patients subjected to electromagnetic fields with f=1 Hz (blue) and 50 Hz (red).

signals so that they have the same baseline, the cross-correlation method was used. This method finds the time shift between two signals that maximizes their similarity. Following are some examples of the graphs obtained (Figures 4.36 - 4.38).

If we compare the effect of different applied frequency of electromagnetic field, we can note that if the frequency is increased, the temporal shift occurs. Even if at the beginning two signals almost coincided, the further you go in time, the more the higher frequency signal delays. Furthermore, it is possible to observe that also the R peaks undergo variations.

Then the phase maps were analyzed (Appendix A, Listing A.6). Phase maps constructed as voltage in function of the derivative of voltage in an ECG signal can provide insights into the dynamics and relationships between voltage changes and their rate of change (slope) (Figures 4.39 - 4.41).

Then the recursive maps were obtained (Appendix A, Listing A.7). Creating a recursive map of an ECG signal involves plotting the voltage at each time step against the voltage at the previous time step (Figures 4.42 - 4.44). This can reveal certain dynamics or patterns in the signal over time.

Finally, the plots with systolic blood pressure were constructed (Figures 4.45 - 4.49).

The shape and the amplitude of the plots seem to be similar for the frequencies from 1 Hz to 245 Hz applied to patients. After 245 Hz the shape changes drastically and become square wave (Figures 4.48 and 4.49).

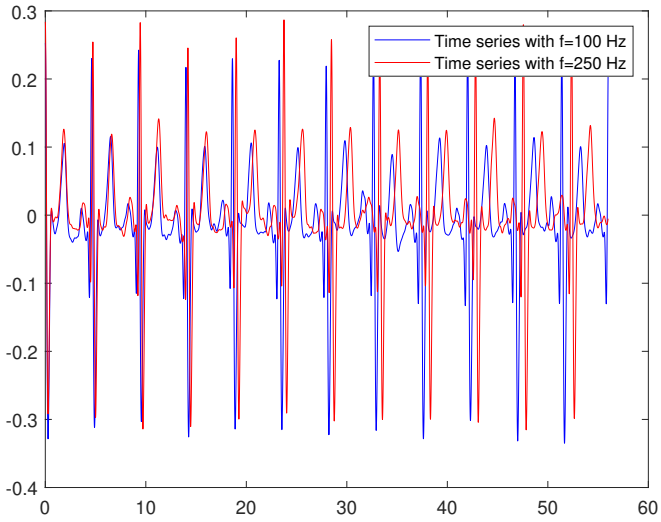

Figure 4.37: Time series obtained from data of patients subjected to electromagnetic fields with f=100 Hz (blue) and 250 Hz (red).

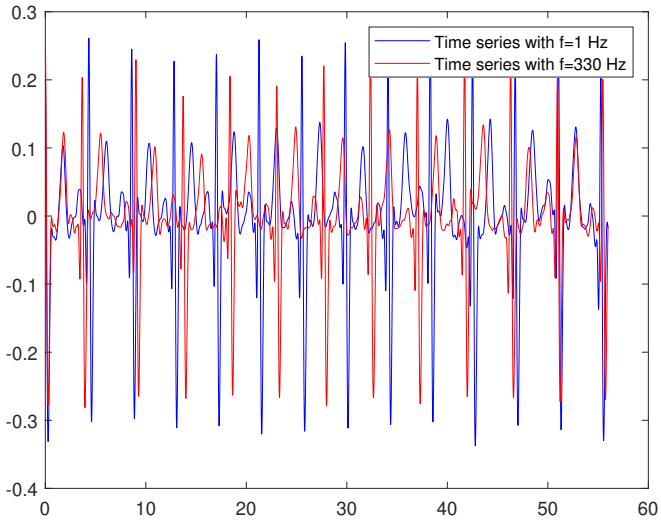

Figure 4.38: Time series obtained from data of patients subjected to electromagnetic fields with f=1 Hz (blue) and 330 Hz (red).

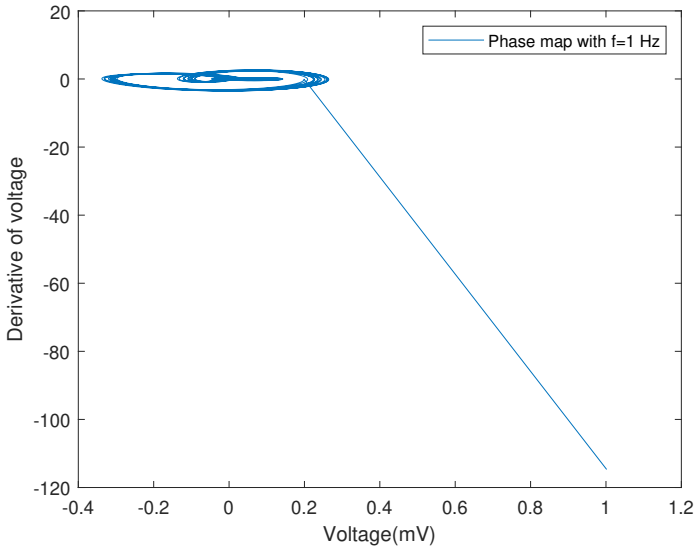

Figure 4.39: Phase map obtained from data of patients subjected to electromagnetic fields with f=1 Hz.

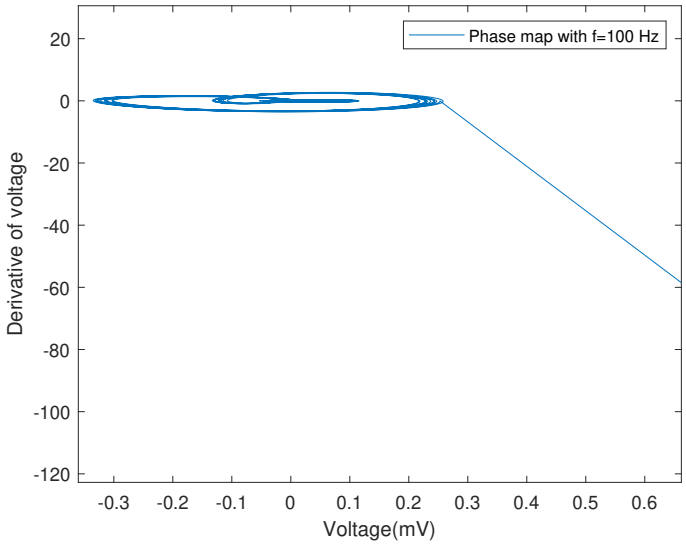

Figure 4.40: Phase map obtained from data of patients subjected to electromagnetic fields with f=100 Hz.

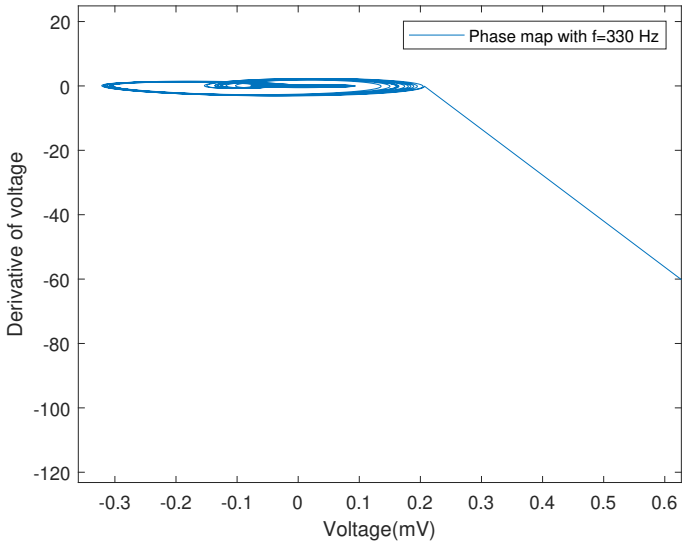

Figure 4.41: Phase map obtained from data of patients subjected to electromagnetic fields with f=330 Hz.

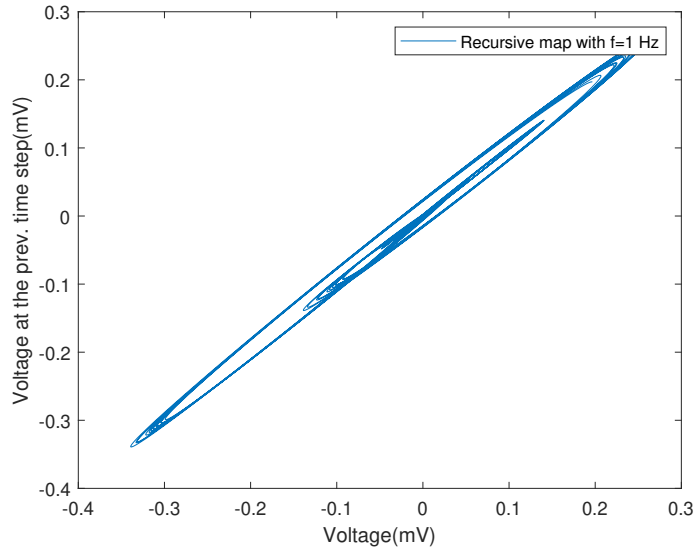

Figure 4.42: Recursive map obtained from data of patients subjected to electromagnetic fields with f=1 Hz.

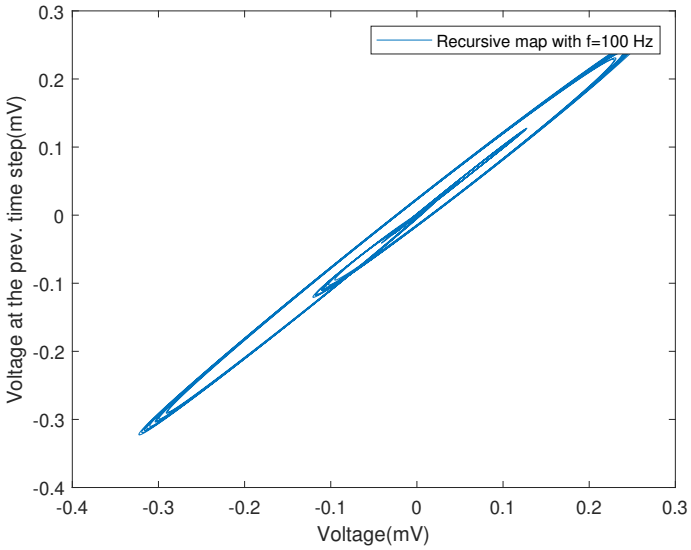

Figure 4.43: Recursive map obtained from data of patients subjected to electromagnetic fields with f=100 Hz.

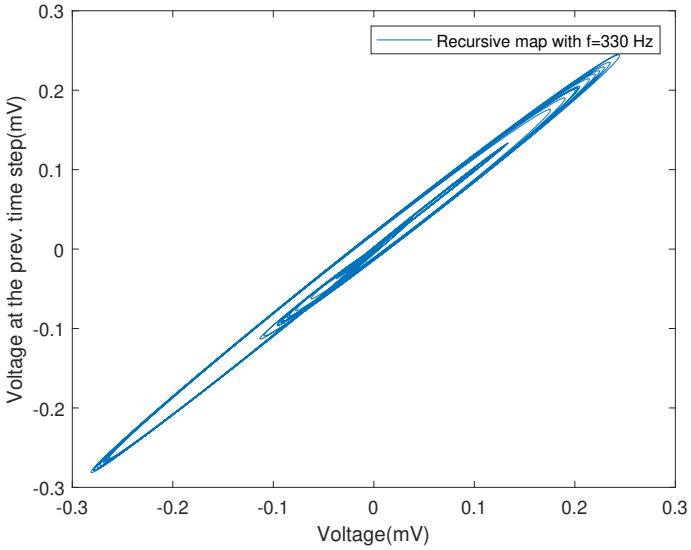

Figure 4.44: Recursive map obtained from data of patients subjected to electromagnetic fields with f=330 Hz.

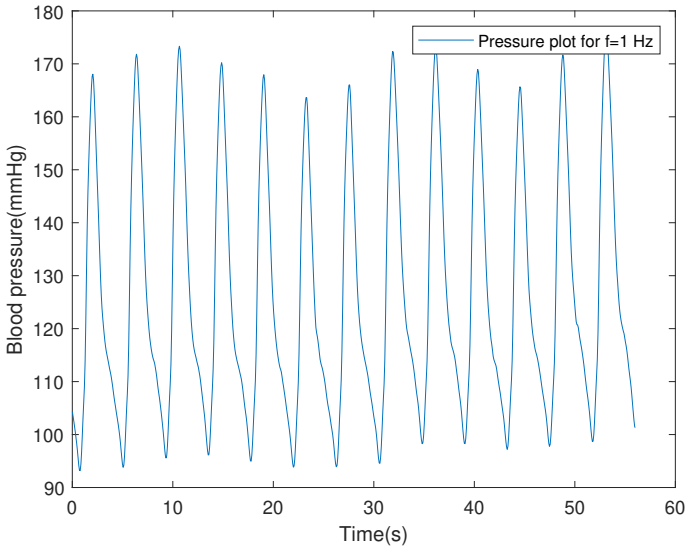

Figure 4.45: Plot of systolic blood pressure obtained from data of patients subjected to electromagnetic fields with f=1 Hz.

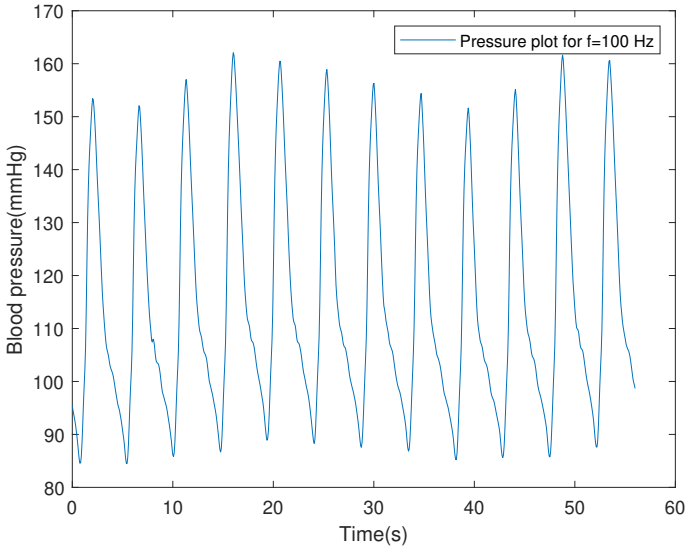

Figure 4.46: Plot of systolic blood pressure obtained from data of patients subjected to electromagnetic fields with f=100 Hz.

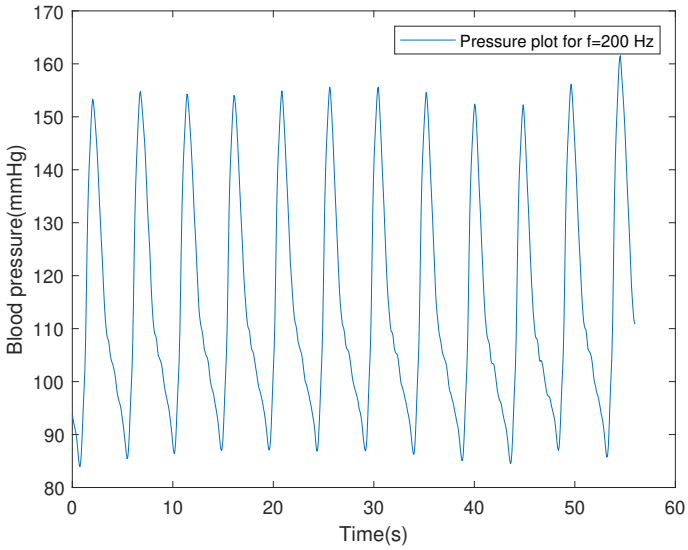

Figure 4.47: Plot of systolic blood pressure obtained from data of patients subjected to electromagnetic fields with f=200 Hz.

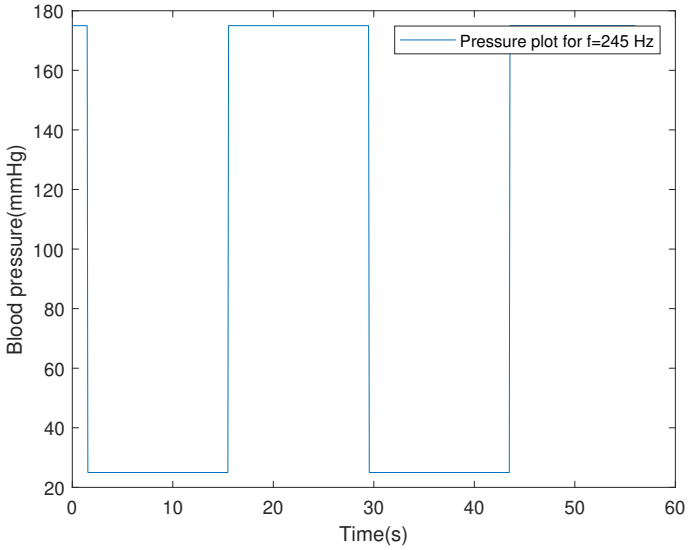

Figure 4.48: Plot of systolic blood pressure obtained from data of patients subjected to electromagnetic fields with f=245 Hz.

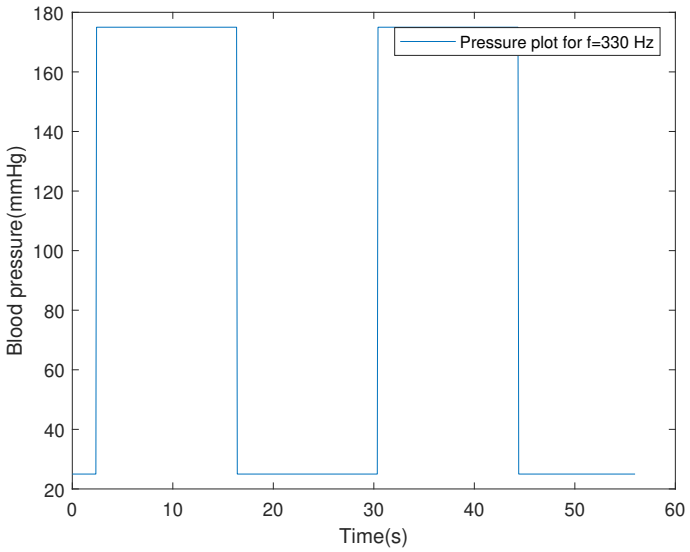

Figure 4.49: Plot of systolic blood pressure obtained from data of patients subjected to electromagnetic fields with f=330 Hz.

4.3 Blood pressure model

To construct the Windkessel model, utilized to explain how blood pressure and blood flow interact throughout the vascular system, the parameters like resistance and compliance are needed. It was decided to create the two-element model (3.1). In this model, the blood flow from the ventricle into the aorta during the cardiac cycle is denoted by $I(t)$. $I(t)$ is a sine wave that has amplitude I_0 during systole and 0 outside of it. Since the ventricles are relaxed during diastole, there is no blood flow into the aorta, and $I(t) = 0$. Blood is expelled into the aorta during ventricular contraction during systole, though, and this process can be represented as a sinusoidal wave [56]:

$$I(t) = I_0 sin(\pi * \frac{mod(t, T_c)}{T_s}) \tag{4.20}$$

where t is time in seconds, T_c is the period of cardiac cycle in seconds, T_s is the systolic period in seconds and $mod(t, T_c)$ is the amount left behind after dividing t by T. Based on the cardiac cycle's dynamics, T_s results to be $\frac{2}{5}T_c$. In general, the average adult heart pumps about 5 liters of blood per minute at rest, which equates to about 70-80 milliliters of blood per beat. So in one cardiac cycle, if the duration of a cardiac cycle is typically between 0.6 to 1 second, the volume of blood flow is equal to $\approx 90cm^3$. To find the maximum value of amplitude during systole I_0, it's necessary to solve the integral (Appendix A, Listing A.8):

$$90 = \int_0^{T_c} I_0 sin(\pi * \frac{mod(t, T_c)}{T_s}) dt \tag{4.21}$$

The solution is $135 * \pi$ mL equal to 424.1 mL [56]. The aortic blood flow of three cardiac cycles with $T_c = 60/72$ s and $T_s = 2/5T_c$ can be represented in Figure 4.50 (Appendix A, Listing A.9). Aortic blood flow can vary depending on factors such as cardiac output, heart rate, and the condition of the cardiovascular system. However, a flow rate of 423 ml/s suggests efficient circulation and adequate perfusion of the body's tissues and organs.

As mentioned before (3.1), the value of blood flow depends on parameters C and R. So during the systolic phase:

$$\frac{dP(t)}{dt} + \frac{P(t)}{CR} = I(t) \tag{4.22}$$

If the integrating factor $u(t) = \int \frac{1}{CR} dt = e^{\frac{t}{RC}}$ is used, the equation 4.22 becomes:

$$\frac{dP(t)}{dt} e^{\frac{t}{RC}} + e^{\frac{t}{RC}} \frac{P(t)}{CR} = \frac{I_0}{C} sin(\pi t / T_s) e^{\frac{t}{RC}} = \frac{d}{dt}(e^{\frac{t}{RC}} P(t)) \tag{4.23}$$

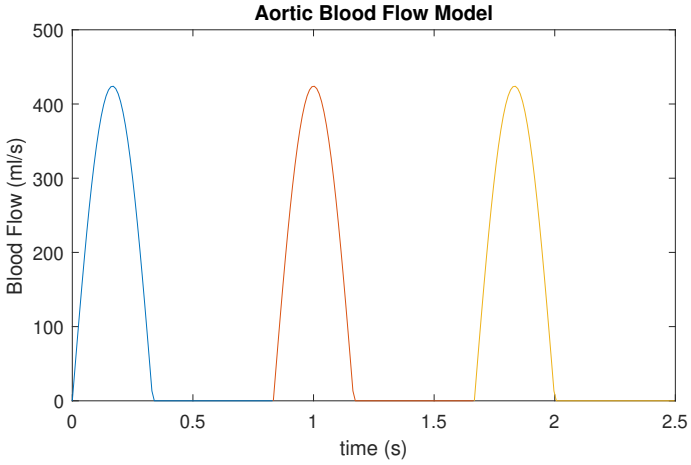

Figure 4.50: Model of aortic blood flow for three cardiac cycles.

Integrating both sides of the equation 4.23:

$$\int d(e^{\frac{t}{RC}} P(t)) = \int \frac{I_0}{C} sin(\pi t/T_s) e^{\frac{t}{RC}} dt \tag{4.24}$$

The solution of this equation is:

$$y(t) = c_1 e^{\frac{-t}{RC}} + \frac{-e^{\frac{t}{CR}} T_s I_0 R(C\pi R cos(\frac{\pi t}{T_s}) - T_s sin(\frac{\pi t}{T_s}))}{T_s^2 + C^2\pi^2 R^2} \tag{4.25}$$

Since systole is preceded by diastole, the initial condition of the systolic phase is the diastolic pressure P_{ss} (pressure of start of systolic cycle). So the solution of constant c_1 becomes:

$$c_1 = P_{ss} + \frac{I_0 T_s R[C\pi R]}{T_s^2 + C^2\pi^2 R^2} \tag{4.26}$$

Meanwhile during the diastole phase, as mentioned before, $I(t) = 0$ and

$$P(t) = ce^{\frac{-t}{RC}} \tag{4.27}$$

The initial condition to find the c constant value is the pressure of the end of systolic phase P_{sd} (pressure of start of diastolic phase). To plot the systolic and diastolic pressure trend, the values of parameters are needed (Appendix A, Listing A.10). The main parameters for two-element model are systemic peripheral resistance $R = 0.95\frac{mmHg}{cm^3}sec$ and systemic arterial compliance $C = 1.0666\frac{cm^3}{mmHg}$ [57]. The plot of systolic and diastolic pressure is represented in Figure 4.51.

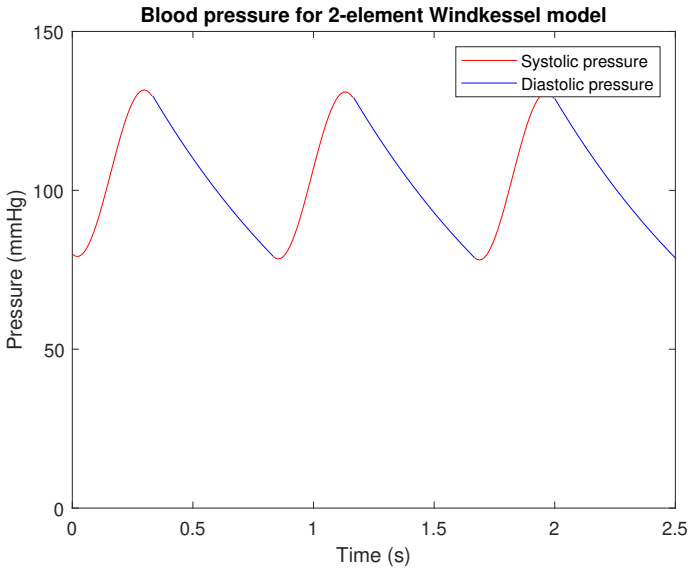

Figure 4.51: Model of blood pressure during three cardiac cycles.

Chapter 5

Results and discussion

5.1 Influence of solutions by parameters

After the construction of HRV and blood pressure models, it is possible to analyze the results obtained. As seen previously, Van der Pol model solutions are sensitive to different parameter values. The solution of VdP equation shows oscillating activity that reflects the contraction and relaxation cycle of the heart during the heartbeat. In case when the forcing term is absent and when we use the original Van der Pol equation, the parameter μ has a huge impact on the outcome. In particular, when $\mu = 0$, the harmonic oscillations are obtained (Figure 4.1). Increasing μ values, the system tends to slow down the oscillations of the system. This effect is due to the greater dissipative force introduced by the parameter, which reduces the system's ability to oscillate rapidly (Figures 4.2-4.4). Furthermore, at higher values of μ , the system can become more stable around its equilibrium point. This may mean that the system tends to return to its steady state more quickly after being perturbed as shown in phase plots of Figures 4.2-4.4. As for the power spectral density, if the μ value increases, the oscillations slow down. As a result, peak frequencies in the power spectrum may decrease, since the system is not able to oscillate as rapidly as at lower values of μ as seen in power spectral density graphs of Figures 4.2-4.4.

Unfortunately, the original Van der Pol equation must be modified to better represent cardiac variability by introducing additional terms that capture specific phenomena of the cardiovascular system. In this way, also the parameters as α, ν_1, ν_2, d and e influence the solution of modified Van der Pol equation. Parameter α determines the strength of the nonlinear effect in the equation. Larger α values indicate greater complexity and dynamism in the cardiovascular system, which could be reflected in heart rate variability. From the Figure 4.7-4.9 it is possible to note that when the α value increases, raises the strength of non-linear terms in

the equation, which may lead to a more non-linear systemic behavior. This can cause increased sensitivity to changes in system parameters and initial conditions. Increasing α leads to a change in the frequency of the oscillations (the frequency decreases) meanwhile the amplitude seems to remain the same. In the phase map, the parameter increase affects the shape and arrangement of the transitory elements, which graphically depicts the system's evolution over time in terms of its state variables. ν_1 and ν_2 are the parameters that influence the position of the equilibrium points in the phase plane. These parameters could be interpreted as reference values or threshold levels that influence the activation of control mechanisms in the cardiac system. Their values could reflect adaptations in the cardiovascular system in response to external stimuli or changes in physiological or pathological conditions. Changes in $\nu 1$ and ν_2 values can affect the frequency, amplitude, or shape of oscillations. This can occur because increasing these parameters can alter the strength of the nonlinear terms in the equation, thus affecting the dynamics of the system. From Figures 4.10-4.12 it is feasible to observe that an increase of parameter values leads to the amplitude growth and frequency decrease. Furthermore, the rise of ν_1 and ν_2 affects the stability of the equilibrium points. As the value increases, the equilibrium points become more stable. d and e parameters could be associated with external factors that influence the dynamics of the cardiac system. When the value of d parameter decreases, the oscillation frequency decreases drastically (Figures 4.13-4.15). The limit cycle becomes more narrow, it suggests that the system exhibits greater local stability around the equilibrium points. From the figures 4.16-4.18 it is clear that also the parameter e influences che behavior of the oscillations. In particular, when its value increases, the oscillation frequency grows, meanwhile the limit cycle of the phase maps seems to remain invariable. This can mean that oscillatory behavior of the system, represented by that limit circle, is robust to variations in the parameter e.

The values of parameters discussed previously were taken from the work of Grudzinski et al. (2004) [54]. The solutions with these parameters were compared with solutions obtained with parameters extracted through use of Genetic Algorithm by the group of Lopez-Chamorro et al. (2018) [55]. From Figures 4.6 and 4.19 it is possible to observe the drastic changes. As mentioned before, the results obtained with parameters from Table 4.1 represent better the shape of action potentials captured from a cardiac pacemaker's real cells (Figure 4.20). The amplitude in this case is larger but oscillation frequency is lower compared to case of Figure 4.6. Furthermore, the limit cycle of Figure 4.19 is very narrow and elongated. This can indicate robust stability of the system with respect to perturbations because the system is able to oscillate in a coherent and predictable way over time, maintaining a certain distance from unstable equilibrium points. Also in this case the increase of α parameter leads to the decrease of oscillation frequency, meanwhile the amplitude and the shape remain the same (Figures 4.20 and 4.21). Furthermore, when α

value increases, the limit cycle stretches. This could mean increasing stability as the orbits stay closer to the equilibrium point for a longer period of time before diverging. The oscillation frequency decreases also if the ν_1 and ν_2 values increase (Figures 4.22 and 4.23). Moreover, the more elongated and wider shape of limit cycle indicates that as the value of parameters increase, increases also the amplitude. The oscillation frequency is influenced also by the parameter d. When it increases, the oscillation frequency increases too, meanwhile the amplitude and the limit cycle remain the same (Figures 4.24 and 4.25). Finally, the increase of oscillation frequency is due to the increase of e value (Figures 4.26 and 4.27). Also in this case, the amplitude and the cycle limit seem to remain unchanged.

The application of the external force leads to big changes of the solutions of VdP equation. If the forcing term is represented by a sinusoid and if the amplitude A of the force increases,the intensity of the external perturbation applied to the system increases too. It leads to the increase of oscillation amplitude, the oscillation regime of the system is disturbed, resulting in a variation in the period and shape of the oscillations (Figures 4.32 and 4.33). The increase in the amplitude of the external force also leads to non-linear phenomena such as the appearance of new harmonics, the instability of the system and the presentation of chaotic behaviors. Furthermore, the trajectories in the phase plane widen, the limit cycle, which represents the periodic orbit in the phase plane, expands, the orbits are more intricate. The increase in pulsation ω leads to a change in the frequency of the external force applied to the system. It is possible to note from Figures 4.30 and 4.31 how the oscillation frequency decreases as the pulsation ω declines. Moreover, when the ω value increases, the improvement of periodicity in the system occurs. This phenomenon is particularly evident when the natural frequency of the system is close to the frequency of the applied external force. Furthermore, the increase in ω leads to a change in the shape and size of the trajectories in the phase plane, causing distortions of existing trajectories.

As demonstrated previously, if the electromagnetic field is applied to the system, the modified VdP equation becomes:

$$x'' + \alpha(x - \nu_1)(x - \nu_2)x' + \frac{x(x + d)(x + e)}{de} = Asin(\omega t)[1 + sin(ft)] \qquad (5.1)$$

where ω is a carrier wave frequency and f is tumor specific envelope frequency. To establish the possible value of the amplitude A, estimates of parameters as conductivity of myocardium, voltage experienced by the heart, cross-sectional heart area and time constant were taken into account. From the Figure 4.35 it is possible to note that the time series results to be not periodic and chaotic. Probably, the presence of a modulated sine wave can cause resonance and beat frequency phenomena that contribute to the complexity of the system and the generation of an aperiodic time series. Even if the system is sensitive to initial

conditions, small variations in initial conditions can lead to divergent behavior over time, contributing to the generation of an aperiodic time series. Another reason could be the inaccurate approximation of parameters as the amplitude of the electromagnetic signal or the time constant. Regarding the time constant, it would be much better to know the value of $\frac{R}{L}$, that is, the relationship between the resistance and inductance of the heart in response to the application of the magnetic field.

5.2 Data analysis

The application of a low-frequency electromagnetic field affects the ECG in several ways, but it mainly depends on the strength of the electromagnetic field, the duration of exposure and the sensitivity of the ECG measuring equipment. External electromagnetic fields can introduce interference into the electrical signal measured by the heart. This may cause artifacts or distortions in the ECG trace, making it more difficult to interpret the signal correctly. If the electromagnetic field has enough energy to directly affect the heart, it could cause changes in heartbeats. This may be reflected in the ECG tracing, showing abnormalities or irregularities in heart signals. From the patient data it is possible to observe how ECG signal, phase map and recursive map change by the application of the electromagnetic field. If the frequency of stimulation increases, the temporal shift occurs (Figures 4.36 - 4.38). This phenomenon is known as "conduction delay". When the pacing rate is high, the heart may not have enough time to complete the refractory period before the next pacing. As a result, the conduction of the electrical signal delays. As regards the phase map, from the Figures 4.39 - 4.41 it is possible to see that as the frequency value increases, the limit cycle shortens not very significantly. If the electromagnetic field strength becomes high enough to significantly interfere with the ECG signal, signal distortion occurs which makes it more difficult to clearly identify the various phases of the cardiac cycle on the phase map. In other words, the area in which the ECG signal can be correctly interpreted may become smaller, leading to a shorter "limit cycle." The presence of a limit cycle in recursive maps (Figures 4.42 - 4.44) may indicate that the system has reached a state of stable equilibrium or periodic oscillation. From the plots of systolic blood pressure (Figures 4.45 - 4.49) obtained from patient data it is possible to observe that when the frequency of electromagnetic field exceeds 245 Hz, the square wave is obtained. At higher frequencies, the cardiovascular system may reach a saturation point where its ability to respond to changes in pressure is limited. This may affect the shape of the systolic pressure wave, making it more "flat" or "square." Furthermore, at higher frequencies, distortions in the systolic pressure signal may occur due to technical factors or artifacts in data acquisition. It is important to make evident that the

results obtained do not represent reality, as noise and unwanted interference may be present in the signal. It is not possible to completely remove noise from an ECG signal. External electromagnetic fields, such as those produced by electronic devices, household appliances, or other medical equipment, can interfere with the ECG signal. This interference may occur due to the physical proximity of the device to the patient or to the ECG signal acquisition device.

5.3 Windkessel model analysis

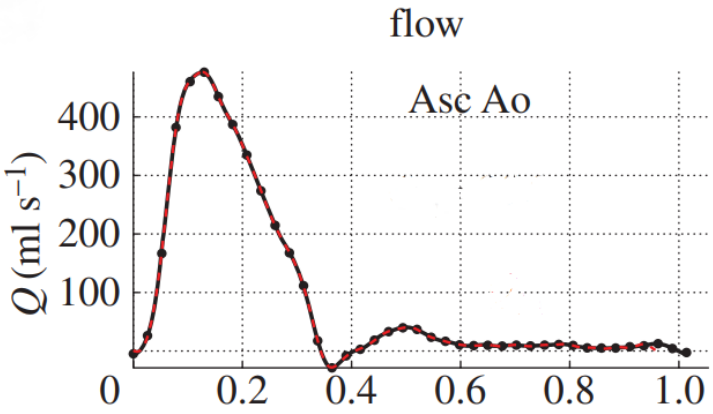

Figure 5.1: Blood flow waveform measured by PC-MRI in one cardiac cycle.

The graph of the Figure 4.50 confirms that maximum amplitude value during systole I_0 obtained from the assumption that the volume of blood flow in one cardiac cycle is about $90cm^3$, could be reasonable. Aortic blood flow can vary depending on factors such as cardiac output, heart rate, and the condition of the cardiovascular system. However, a flow rate of 423 ml/s suggests efficient circulation and adequate perfusion of the body's tissues and organs. This flow rate is indicative of a healthy cardiovascular system with a normal cardiac output. It's within the range of typical blood flow rates observed in the aorta during rest and moderate activity in healthy adults. Also the work of Alastruey et al. (2016) affirms the correctness of results. In Figure 5.1 [58] the blood flow waveform measured by phase contrast magnetic resonance imaging (PC-MRI) is represented. If this figure is compared to Figure 4.50, it is possible to note the similarity both in the shape and amplitude of the waves. The resulting model of blood pressure (Figure 4.51) also seems to have reasonable values of maximum and minimum amplitudes because a healthy person's systolic and diastolic blood pressure are approximately 120 and 80 mmHg, respectively. This value can vary slightly depending on factors

such as age, gender, and overall health.

The two-element model proposed is incomplete. As mentioned before, three- and four-element models could better describe cardiac hemodynamics and aim to capture more complexities in arterial properties. The three-element model represents the arterial system as a lumped model with compliant arteries that store and release blood during the cardiac cycle, resistance to flow offered by the arterioles, and inertial effects due to the pulsatile nature of blood flow. Meanwhile in the four-element model, the addition of systemic vascular resistance represents the combined resistance of the systemic vasculature beyond the arterioles, including the resistance offered by the capillaries and veins.

Chapter 6

Conclusion

Heart's intricate electrical conduction system plays a vital role in regulating its rhythmic pumping action. From the initial stimulation of the sinoatrial (SA) node to the coordinated contraction and relaxation of the atria and ventricles, each step in the cardiac cycle ensures efficient blood circulation throughout the body. The measurement of heart rate variability (HRV) has emerged as a valuable tool for assessing autonomic nervous system function and predicting prognosis in various medical conditions, including cancer. Studies have shown that decreased HRV is associated with tumor growth and poorer outcomes in cancer patients, highlighting its potential as a prognostic indicator. Additionally, research on the effects of low-energy amplitude-modulated radiofrequency electromagnetic fields suggests a potential therapeutic role in slowing cancer cell growth. Understanding the complex interplay between cardiac function, HRV, and cancer biology holds promise for improving patient care and treatment outcomes in oncology. Further investigation into these areas is warranted to harness the full potential of cardiac physiology and electromagnetic therapies in managing cancer and other related conditions.

The analysis of heart rate variability encompasses various measures and methodologies, each providing unique insights into the autonomic nervous system's modulation of cardiac activity. Time-domain measures, such as standard deviation of NN intervals (SDNN) and root mean square of successive NN interval differences (RMSSD), offer information about variability over different time intervals, while frequency-domain measures, including low frequency and high frequency power, correlate HR oscillations with sympathetic and parasympathetic activity, respectively. Furthermore, nonlinear measures, such as Poincaré plot descriptors and Lyapunov exponents, provide valuable insights into the complexity and dynamics of HRV, offering potential for enhanced risk stratification and diagnostic capabilities. The exploration of HRV through mathematical modeling, particularly using the Van der Pol equation, offers a theoretical framework for understanding cardiac oscillatory behavior, aiding in the interpretation of experimental findings and guiding future

research directions. Overall, the integration of diverse measures and methodologies in HRV analysis holds promise for advancing our understanding of autonomic regulation of the heart, facilitating improved risk assessment, diagnostic accuracy, and therapeutic interventions in various cardiovascular conditions.

Windkessel model provides a valuable framework for understanding cardiovascular hemodynamics, particularly the interaction between blood pressure, resistance, and cardiac output. Originating from Otto Frank's work in 1899, this model has evolved from the simple two-element version to more complex iterations, such as the three-element and four-element models, to better capture the dynamics of arterial flow and pressure. The Windkessel effect, illustrated by the analogy of a hydraulic pump with an air chamber, elucidates how arterial compliance and peripheral resistance influence arterial blood pressure waveforms during cardiac cycles. By incorporating factors like arterial compliance, peripheral resistance, and the resistance caused by valves, the Windkessel model offers insights into physiological phenomena like systole and diastole, arterial stiffness associated with aging, gender differences, and the impact of diseases like hypertension and atherosclerosis on arterial elasticity. Moreover, hypertension often coexists with cancer, with renal cell carcinoma being the most consistently linked cancer type. Studies suggest potential positive associations between hypertension and various other cancers, though the exact biological mechanisms remain unclear. The treatment of hypertension, particularly with angiogenesis inhibitors in cancer therapy, poses additional cardiovascular risks, emphasizing the importance of managing blood pressure effectively in patients undergoing oncologic treatment.

By employing the two-element model, which considers parameters such as resistance and compliance, we can simulate the interaction between blood pressure and flow during the cardiac cycle. The model represents blood flow from the ventricle into the aorta during systole as a sinusoidal wave, with no flow during diastole. By solving for the maximum amplitude of blood flow during systole, we can estimate the volume of blood ejected into the aorta per beat. This estimation, coupled with parameters such as cardiac cycle duration and systolic period, allows us to construct a model of aortic blood flow over multiple cardiac cycles. Furthermore, by considering the dynamics of pressure during systole and diastole, we can derive differential equations that describe the changes in pressure over time. These equations, along with appropriate initial conditions, enable us to plot the trends of systolic and diastolic pressures throughout the cardiac cycle. Utilizing parameters such as systemic peripheral resistance and systemic arterial compliance, we can generate plots that illustrate the fluctuations in blood pressure during successive cardiac cycles. These plots provide valuable insights into the dynamics of blood pressure regulation and the efficiency of cardiovascular function.

The computational modeling of heart rate variability in cancer patients using

nonlinear differential equations, particularly the Van der Pol oscillator, offers valuable insights into the complex dynamics of the autonomic nervous system and cardiovascular system. Through sensitivity analysis of model parameters, such as the damping parameter μ, it was observed that variations in these parameters significantly affect the behavior of the oscillator, influencing oscillation frequency, amplitude, and stability. The sensitivity of solutions to initial conditions further underscores the importance of understanding the precise starting conditions for accurately predicting system behavior. Additionally, the modification of the Van der Pol equation to better model cardiac activity, as demonstrated by incorporating parameters such as α, ν_1, ν_2, d, and e, provides a more nuanced representation of heart dynamics. This modified model allows for the simulation of phenomena like refractory periods and spontaneous depolarization, which are crucial in understanding cardiac function. Furthermore, the introduction of a sinusoidal forcing term into the modified Van der Pol equation offers a means to model external influences on cardiac activity, such as electromagnetic fields. The determination of appropriate parameter values, considering factors like current density, conductivity, and time constants, enables the accurate representation of real-world scenarios. These simulations not only deepen our understanding of cardiac dynamics but also provide insights into the effects of external stimuli on heart function.

The analysis of the patient database provided by Hospital Sirio Libanes offered valuable insights into the effects of electromagnetic fields on physiological parameters, particularly electrocardiogram signals and blood pressure. The preprocessing of ECG signals involved detrending to correct baseline shifts caused by patient movement, followed by the measurement of ECG gradients and systolic blood pressure. The time series plots revealed distinct temporal shifts and variations in ECG waveforms, particularly noticeable with increasing frequencies of electromagnetic field application. The phase maps provided further insights into the dynamics of voltage changes and their derivatives, suggesting different patterns of signal behavior across frequencies. Recursive maps demonstrated the relationships between voltage values at consecutive time steps, offering a visualization of signal dynamics over time. Notably, the plots of systolic blood pressure exhibited consistent shapes and amplitudes for frequencies ranging from 1 Hz to 245 Hz, indicating a similar physiological response within this frequency range. However, beyond 245 Hz, there was a notable deviation in the shape of the blood pressure waveform, resembling a square wave pattern. Overall, these analyses highlight the complex interplay between electromagnetic field frequencies and physiological parameters, providing a foundation for further investigation into the effects of electromagnetic fields on cardiovascular health.

To make the models more complete, it is possible to think about the addition of the new terms. For example, the HRV model can be represented by three oscillators

(sinoatrial node, atrioventricular node and His-Purkinje complex) paired with time-delayed terms that show the amount of time each oscillator spends transmitting. This modification improves the model's ability to explain diseases that are based on observations of specific pathological behaviors, such as atrial fibrillation and flutter. Furthermore, in addition to parameters like resistance and compliance, it is possible to include the characteristic impedance and characteristic time τ to obtain three- or four-element Windkessel model. Characteristic impedance represents the impedance of the arterial system, meanwhile characteristic time represents the time constant of the system. The three- and four-element model generally provide a more accurate representation of arterial dynamics, especially in scenarios involving wave propagation and reflections. Moreover, one of the future works can be the fitting of Van der Pol and Windkessel models to patient data. The goal of this future work will be the definition of objective function that quantifies the mismatch between model predictions and observed data and then the research of optimization techniques (such as gradient-based methods, genetic algorithms, or Bayesian approaches) to find the set of model parameters that minimize the objective function.

Appendix A

MATLAB scripts

```
clc
close all
clear variables

% constant initial conditions, different values of mu

mu=0; % nonlinear term,indicates the strength of the damping
x0=1;
v0=0;
t=0:0.001:60;    % time scale

figure(1)
[x_1]=my_vanderpol(mu,t,x0,v0);

figure(2)
mu=0.1;
[x_2]=my_vanderpol(mu,t,x0,v0);

figure(3)
mu=1;
[x_3]=my_vanderpol(mu,t,x0,v0);

figure(4)
mu=3;
[x_4]=my_vanderpol(mu,t,x0,v0);

function [x]=my_vanderpol(mu,t,x0,v0)

k=1;
[t,x] = ode45(@rhs,t,[x0,v0]);

subplot(3,1,1);
plot(t,x(:,1));
```

```
xlabel('t');
ylabel('x(t)');
title_mu=sprintf('%3.2f',mu);
plot1_title=strcat('Position vs time with mu=',title_mu);
title(plot1_title);

subplot(3,1,2);
plot(x(:,1),x(:,2));
xlabel('x(t)');
ylabel('v(t)');
hold on;
plot(x0,v0,'*r','MarkerSize',10);
title_x0=sprintf('%3.2f',x0);
title_v0=sprintf('%3.2f',v0);
plot2_title=strcat('Phase map with x0=',title_x0, ' and v0= ',
    title_v0);
title(plot2_title);

% title('Phase map with x(0)=%3.2f, v(0)=%3.2f',x0,v0);
axis equal
hold on;

% PSD(Power Spectral Density) describes how the power of the
    signal is distributed across different frequency bands

fs=200;
N=length(t); % length of the signal
window=hanning(N);
[Pxx, f] = pwelch(x(:,1), window, [], [], fs);

subplot(3,1,3);
plot(f, 10*log10(Pxx)); % convert to dB for better visualization
xlabel('Frequency (Hz)');
ylabel('Amplitude (dB)');
plot_psd=strcat('Power Spectral Density for mu=',title_mu,' ,x0= '
    ,title_x0,' and v0= ',title_v0);
title(plot_psd);
hold off;

    function dxdt=rhs(t,x)
        dxdt_1 = x(2);
        dxdt_2 = mu*(1-x(1)^2)*x(2)-k*x(1);

        dxdt = [dxdt_1 ; dxdt_2];
    end
end
```

Listing A.1: MATLAB script for the analyses of parameter sensitivity of solutions of Van der Pol equation.

```
clc
close all
clear variables

% Define the modified Van der Pol equation
%trial 1
alpha = 5.5982; % Set the value of the parameter alpha
nu1 = 2.5151; % Set the value of the parameter nu1
nu2 = -2.5151; % Set the value of the parameter nu2
d = 10.6335; % Set the value of the parameter d
e = 10.0548; % Set the value of the parameter e

%trial 2
% alpha = 5.5982;
% nu1 = 2.5151;
% nu2 = -2.5151;
% d = 10.6335;
% e = 10.0548;

%trial 3
% alpha = 5.5982;
% nu1 = 2.5151;
% nu2 = -2.5151;
% d = 10.6335;
% e = 10.0548;

%trial 4
% alpha = 5.5982;
% nu1 = 2.5151;
% nu2 = -2.5151;
% d = 10.6335;
% e = 10.0548;

% Define a time span
t=0:0.001:60;

% Define initial conditions
x0 = 1; % Initial displacement
v0= 0; % Initial velocity

% Solve the ODE
ode = @(t, x) [x(2); -alpha*(x(1)-nu1)*(x(1)-nu2)*x(2) - x(1)*(x
    (1)+d)*(x(1)+e)/e];
[t, x] = ode45(ode, t, [x0,v0]);

% Plot the time series
subplot(3,1,1);
plot(t,x(:,1));
```

```
xlabel('t');
ylabel('x(t)');
title_alpha=sprintf('%3.2f',alpha);
title_nu1=sprintf('%3.2f',nu1);
title_nu2=sprintf('%3.2f',nu2);
title_d=sprintf('%3.2f',d);
title_e=sprintf('%3.2f',e);
plot1_title=strcat('Position vs time with alpha= ',title_alpha,', v1= ',title_nu1,', v2= ',title_nu2,', d= ',title_d,' and e= ', title_e);
title(plot1_title);

% Plot the phase portrait
subplot(3,1,2);
plot(x(:, 1), x(:, 2));
xlabel('Displacement (x)');
ylabel('Velocity (dx/dt)');
hold on;
title_x0=sprintf('%3.2f',x0);
title_v0=sprintf('%3.2f',v0);
plot(x0,v0,'*r','MarkerSize',10);
plot2_title=strcat('Modified Van der Pol Oscillator Phase Portrait with alpha= ',title_alpha,', v1= ',title_nu1,', v2= ', title_nu2,', d= ',title_d,' and e= ',title_e);
title(plot2_title);
axis equal
hold on;

%Plot power spectral density
fs=200;
N=length(t); % length of the signal
window=hanning(N);
[Pxx, f] = pwelch(x(:,1), window, [], [], fs);

subplot(3,1,3);
plot(f, 10*log10(Pxx)); % convert to dB for better visualization
xlabel('Frequency (Hz)');
ylabel('Amplitude (dB)');
plot_psd=strcat('Power Spectral Density for alpha=',title_alpha,', v1=',title_nu1,', v2=',title_nu2,', d=',title_d,' and e=', title_e);
title(plot_psd);
hold off;
```

Listing A.2: MATLAB script for the analyses of parameter sensitivity of solutions of modified Van der Pol equation.

```
clc
close all
clear variables

% Set the parameters
alpha = 1; % Set the value of the parameter alpha
nu1 = 0.83; % Set the value of the parameter nu1
nu2 = -0.83; % Set the value of the parameter nu2
d = 3; % Set the value of the parameter d
e = 6; % Set the value of the parameter e
A = 2.5; % Set the amplitude of the sinusoidal forcing term
omega = 1.9; % Set the pulsation of the sinusoidal forcing term

% Define a time span
tspan=0:0.001:60;

% Define initial conditions
x0 = [1;0]; % Initial displacement and velocity (v0=0)

% Solve the ODE
[t, x] = ode45(@(t,x) modified_vdp(t, x, alpha, nu1, nu2, d, e, A,
    omega), tspan, x0);

% Plot the time series
subplot(2,1,1);
plot(t,x(:,1));
xlabel('t');
ylabel('x(t)');
title_alpha=sprintf('%3.2f',alpha);
title_nu1=sprintf('%3.2f',nu1);
title_nu2=sprintf('%3.2f',nu2);
title_d=sprintf('%3.2f',d);
title_e=sprintf('%3.2f',e);
title_A=sprintf('%3.2f',A);
title_omega=sprintf('%3.2f',omega);
plot1_title=strcat('Position vs time with A= ',title_A, ', omega=
    ',title_omega, ' alpha= ',title_alpha,', v1= ',title_nu1,', v2=
    ',title_nu2,', d= ',title_d,' and e= ',title_e);
title(plot1_title);

% Plot the phase portrait
subplot(2,1,2);
plot(x(:, 1), x(:, 2));
xlabel('Displacement (x)');
ylabel('Velocity (dx/dt)');
```

```
43 plot2_title=strcat('Modified Van der Pol Oscillator Phase Portrait
       with Forcing Term with A= ',title_A, ', omega= ',title_omega,
   ' alpha= ',title_alpha,', v1= ',title_nu1,', v2= ',title_nu2,',
       d= ',title_d,' and e= ',title_e);
44 title(plot2_title);
45 grid on;
46
47 % Define the modified Van der Pol equation with the forcing term
48 function dxdt = modified_vdp(t, x, alpha, nu1, nu2, d, e, A, omega
   )
49     dxdt = zeros(2,1);
50     dxdt(1) = x(2);
51     dxdt(2) = -alpha*(x(1)-nu1)*(x(1)-nu2)*x(2) - x(1)*(x(1)+d)*(x
   (1)+e)/e + A*sin(omega*t);
52 end
```

Listing A.3: MATLAB script for the analyses of parameter sensitivity of solutions of modified Van der Pol equation with external force.

```
clc
close all
clear variables

% Set the parameters
alpha = 10.5625;
nu1 = 2.596975;
nu2 = -2.596975;
d = 11.548335;
e = 9.9659125;
omega = 27.12*2*pi*10^6;
A_0 = 0.01;
sigma = 0.16;
E_0 = 6.25;
tau = 0.53;
A=A_0*sigma*E_0*omega/tau;
f=2*pi*100;

% Define a time span
tspan=0:0.001:60;

% Define initial conditions
x0 = [1;0]; % Initial displacement and velocity (v0=0)

% Define the system of first-order ODEs
ode = @(t, x) [x(2); -alpha*(x(1)-nu1)*(x(1)-nu2)*x(2) - x(1)*(x
    (1)+d)*(x(1)+e)/(e*d) + A*sin(omega*t)*(1 + sin(f*t))];

% Solve the ODE
[t, x] = ode45(ode, tspan, x0);

% Plot the displacement over time
subplot(2,1,1);
plot(t, x(:, 1));
xlabel('Time');
ylabel('Displacement (x)');
title('Time series of modified VdP oscillator with sinusoidal
    forcing term and electromagnetic field');
grid on;

% Plot the phase portrait
subplot(2,1,2);
plot(x(:, 1), x(:, 2));
xlabel('Displacement (x)');
ylabel('Velocity (dx/dt)');
title('Phase portrait of modified VdP oscillator with sinusoidal
    forcing term and electromagnetic field')
```

Listing A.4: MATLAB script for the analyses of parameter sensitivity of solutions of modified Van der Pol equation with external electromagnetic field applied.

```
close all
clear variables
clc

fileExcel = 'C:\Users\1a3fa385cdb842f4a25d25418e3e385f
    -190846555775244817-1572453016990(1).xlsx';
sheet_work= 'EKG1';
[data, headers, raw] = xlsread(fileExcel, sheet_work);
time=data(:,1);
[row_number,column_number]=size(data);

fs=143; %sampling frequency

% Maximum frequency
max_frequency = data(1,column_number);
max_frequency_str = string(max_frequency);

% Display non-3 frequencies
cnt = 0;
check = zeros(max_frequency,1);
for i=2:column_number-2
    if( (data(1,i) == data(1,i+1)) && (data(1,i+1) == data(1,i+2))
    )
        cnt = cnt+1;
        frequency_checked = data(1,i);
        check(frequency_checked) = 1;
    end
end
fprintf('Non-3 frequencies:\n')
for i=1:335
    if(check(i) == 0)
        fprintf('%d\n', i)
    end
end

prompt1 = 'Insert frequency value from 1Hz to 330Hz to construct
    time series and phase plots: ';
prompt2 = 'Insert frequency value from 1Hz to 330Hz to construct
    time series and phase plots: ';
my_frequency_value_1 = input(prompt1);
my_frequency_value_2 = input(prompt2);
fig_cont=1;
for j=2:column_number
    for k=2:column_number
    frequency_value1=data(1,j);
    frequency_value2=data(1,k);
    if(frequency_value1==my_frequency_value_1) && (
   frequency_value2==my_frequency_value_2)
```

```
44          data_detrend1(:,j)=data(:,j)-mean(data(:,j));
45          data_detrend2(:,k)=data(:,k)-mean(data(:,k));
46          [~, lag] = xcorr(data(:,j), data(:,k));
47          [max_corr, max_index] = max(abs(lag));
48          aligned(:,k) = circshift(data(:,k), [0, lag(max_index)]);
49
50          figure(fig_cont);
51          plot(time,data_detrend1(:,j),'b');
52          hold on;
53          plot(time,aligned(:,k),'r');
54          legend('Time series with f=1 Hz', 'Time series with f=330
        Hz' );
55
56          fig_cont=fig_cont+1;
57       end
58       end
59  end
```

Listing A.5: MATLAB script for the analyses of time series from patient data.

```
close all
clear variables
clc

fileExcel = 'C:\Users\1a3fa385cdb842f4a25d25418e3e385f
    -190846555775244817-1572453016990(1).xlsx';
sheet_work= 'EKG1';
[data, headers, raw] = xlsread(fileExcel, sheet_work);
time=data(:,1);
[row_number,column_number]=size(data);

% Maximum frequency
max_frequency = data(1,column_number);
max_frequency_str = string(max_frequency);

% Display non-3 frequencies
cnt = 0;
check = zeros(max_frequency,1);
for i=2:column_number-2
    if( (data(1,i) == data(1,i+1)) && (data(1,i+1) == data(1,i+2))
    )
        cnt = cnt+1;
        frequency_checked = data(1,i);
        check(frequency_checked) = 1;
    end
end
fprintf('Non-3 frequencies:\n')
for i=1:335
    if(check(i) == 0)
        fprintf('%d\n', i)
    end
end

prompt1 = 'Insert frequency value from 1Hz to 330Hz to construct
    phase plots: ';
my_frequency_value_1 = input(prompt1);

fig_cont=1;
for j=2:column_number
    frequency_value1=data(1,j);

    if(frequency_value1==my_frequency_value_1)
        data_detrend1(:,j)=data(:,j)-mean(data(:,j));

        dv_dt1(:,j) = diff(data_detrend1(:,j))/diff(time(2:3));

        figure(fig_cont),plot(data_detrend1(1:end-1,j),dv_dt1(:,j)
    ),xlabel('Voltage(mV)'),ylabel('Derivative of voltage');
```

```
45
46          legend('Phase map with f=1 Hz');
47
48          fig_cont=fig_cont+1;
49      end
50      end
```

Listing A.6: MATLAB script for the analyses of phase maps from patient data.

```
close all
clear variables
clc

fileExcel = 'C:\Users\1a3fa385cdb842f4a25d25418e3e385f
    -190846555775244817-1572453016990(1).xlsx';
sheet_work= 'EKG1';
[data, headers, raw] = xlsread(fileExcel, sheet_work);
time=data(:,1);
[row_number,column_number]=size(data);

% Maximum frequency
max_frequency = data(1,column_number);
max_frequency_str = string(max_frequency);

% Display non-3 frequencies
cnt = 0;
check = zeros(max_frequency,1);
for i=2:column_number-2
    if( (data(1,i) == data(1,i+1)) && (data(1,i+1) == data(1,i+2))
    )
        cnt = cnt+1;
        frequency_checked = data(1,i);
        check(frequency_checked) = 1;
    end
end
fprintf('Non-3 frequencies:\n')
for i=1:335
    if(check(i) == 0)
        fprintf('%d\n', i)
    end
end

prompt1 = 'Insert frequency value from 1Hz to 330Hz to construct
    phase plots: ';
my_frequency_value_1 = input(prompt1);

fig_cont=1;
for j=2:column_number
    frequency_value1=data(1,j);

    if(frequency_value1==my_frequency_value_1)
        data_detrend1(:,j)=data(:,j)-mean(data(:,j));

        voltage_t_minus_1=data(2:end-1,j);
        voltage=data(3:end,j);

```

```
45          plot(voltage,voltage_t_minus_1),xlabel('Voltage(mV)'),
    ylabel('Voltage at the prev. time step(mV)');
46
47          legend('Recursive map with f=1 Hz');
48
49          fig_cont=fig_cont+1;
50      end
51      end
```

Listing A.7: MATLAB script for the analyses of recursive maps from patient data.

```
clc
close all
clear variables

%%Asumpltions
Tc= 60/72 ;% 72 beats per second
Ts =(2/5)*Tc ; % systole period
syms ti q
I0= solve(90-int(q *(sin( pi *ti/Ts )),ti,0,Ts),q) ;
I0=subs ( I0 , ' 3.14 ' , pi ) ;
```

Listing A.8: MATLAB script to find the amplitude value of systolic flow.

```
clc
close all
clear variables

% Definition of parameters
Tc = 60/72;       % 72 beats per second
Ts = (2/5)*Tc;    % systole period
cycle = 3;        % number o f cardiac cycles

% Modelling blood flow to the aorta
syms ti q
I0 = solve(90==int(q*(sin(pi*ti/Ts)),ti,0,Ts),q);
I0 = subs(I0,'3.14',pi);
sine = @(t)sin(pi*t/Ts) ;
I = @(t) I0*sine(t).*(t <= Ts) ; % for one cycle
figure (1)

for n=1:cycle
    t=(n-1)*Tc:.01:n*Tc;
    % Blood flow for each cardiac cycle
    I = @(t) I0*sine(t-(n-1)*Tc).*(t <= ((n-1)*Tc+Ts));
    plot(t, I(t));
    hold on
    title('Aortic Blood Flow Model')
    ylabel('Blood Flow (ml/s)')
    xlabel('time (s)')
end
```

Listing A.9: MATLAB script to plot the aortic blood flow.

```
clc
close all
clear variables

% Defining modeling parameters for Windkessel Model
% parameters for 2 element
R = 0.95000;
C = 1.0666;
Tc = 60/72;       % 72 beats per second
Ts = (2/5)*Tc;    % systole period
cycle = 3;        % number of cardiac cycles

%  Modelling blood flow t o the aorta
syms ti q
I0 = solve(90==int(q*(sin(pi*ti/Ts)),ti,0,Ts),q);
I0 = subs(I0,'3.14',pi);
figure (1)

for n=1:cycle
    if n==1
        Pss = 80; %initial condition
    end
    ts=(n-1)*Tc:0.01:(n-1)*Tc+Ts;
    c1= Pss+I0*Ts*R*(C*pi*R)/((Ts^2+C^2*pi^2*R^2));
    Ps= @ (t) c1*exp(-((t-ts(1))/(R*C)))-I0*Ts*R*(C*pi*R*cos( pi*(
   t-ts(1))/Ts)-Ts*sin(pi*(t-ts(1))/Ts))/(Ts^2+C^2*pi^2*R^2);
    Psd=Ps(ts(end));

    td=(n-1)*Tc+Ts:0.01:n*Tc;
    Pd=@(t) Psd*exp(-(t-td(1))/(R*C));
    Pss=Pd(td(end));

    plot(ts, Ps(ts),'r');
    hold on;
    plot(td, Pd(td),'b');
    xlim([0 n*Tc ]);
    ylim([ 0 150]);
    title('Blood pressure for 2-element Windkessel model');
    xlabel('Time (s)');
    ylabel('Pressure (mmHg)');
    legend('Systolic pressure','Diastolic pressure');

end
```

Listing A.10: MATLAB script to plot the systolic and diastolic pressures.

Bibliography

[1] Daniel A Boullosa, José L Tuimil, Anthony S Leicht, and Juan J Crespo-Salgado. «Parasympathetic modulation and running performance in distance runners». In: *The Journal of Strength & Conditioning Research* 23.2 (2009), pp. 626–631 (cit. on p. 3).

[2] Jin-Guo Dong. «The role of heart rate variability in sports physiology». In: *Experimental and therapeutic medicine* 11.5 (2016), pp. 1531–1536 (cit. on p. 3).

[3] Harry Hemingway, Martin Shipley, Eric Brunner, Annie Britton, Marek Malik, and Michael Marmot. «Does autonomic function link social position to coronary risk? The Whitehall II study». In: *Circulation* 111.23 (2005), pp. 3071–3077 (cit. on p. 3).

[4] Marek Malik and A John Camm. «Heart rate variability». In: *Clinical cardiology* 13.8 (1990), pp. 570–576 (cit. on p. 4).

[5] Marek Malik. «Heart rate variability: Standards of measurement, physiological interpretation, and clinical use: Task force of the European Society of Cardiology and the North American Society for Pacing and Electrophysiology». In: *Annals of Noninvasive Electrocardiology* 1.2 (1996), pp. 151–181 (cit. on p. 4).

[6] PK Stein PhD and RE Kleiger MD. «Insights from the study of heart rate variability». In: *Annual review of medicine* 50.1 (1999), pp. 249–261 (cit. on p. 4).

[7] Gustavo A Lopera, Heikki V Huikuri, Timo H Mäkikallio, Jari Tapanainen, Simon Chakko, Raul D Mitrani, Alberto Interian, Agustin Castellanos, and Robert J Myerburg. «Is abnormal heart rate variability a specific feature of congestive heart failure?» In: *American Journal of Cardiology* 87.10 (2001), pp. 1211–1213 (cit. on p. 4).

[8] Marijke De Couck, Boris Mravec, and Yori Gidron. «You may need the vagus nerve to understand pathophysiology and to treat diseases». In: *Clinical science* 122.7 (2012), pp. 323–328 (cit. on pp. 4, 5).

[9] Marijke De Couck and Yori Gidron. «Norms of vagal nerve activity, indexed by Heart Rate Variability, in cancer patients». In: *Cancer Epidemiology* 37.5 (2013), pp. 737–741 (cit. on pp. 4, 5).

[10] Charlotte Mouton et al. «The relationship between heart rate variability and time-course of carcinoembryonic antigen in colorectal cancer». In: *Autonomic neuroscience* 166.1-2 (2012), pp. 96–99 (cit. on pp. 4, 5).

[11] Frank Entschladen, Theodore L Drell, Kerstin Lang, Jan Joseph, and Kurt S Zaenker. «Tumour-cell migration, invasion, and metastasis: navigation by neurotransmitters». In: *The lancet oncology* 5.4 (2004), pp. 254–258 (cit. on p. 5).

[12] Janine Giese-Davis, Frank H Wilhelm, Rie Tamagawa, Oxana Palesh, Eric Neri, Craig Barr Taylor, Helena C Kraemer, and David Spiegel. «Higher vagal activity as related to survival in patients with advanced breast cancer: an analysis of autonomic dysregulation». In: *Psychosomatic medicine* 77.4 (2015), pp. 346–355 (cit. on p. 5).

[13] Nada Fadul, Florian Strasser, J Lynn Palmer, Syed Wamique Yusuf, Ying Guo, Zhijun Li, Julio Allo, and Eduardo Bruera. «The association between autonomic dysfunction and survival in male patients with advanced cancer: a preliminary report». In: *Journal of pain and symptom management* 39.2 (2010), pp. 283–290 (cit. on p. 6).

[14] Ying Guo, Shalini Koshy, David Hui, J Lynn Palmer, Ki Shin, Mehtap Bozkurt, and Syed Wamique Yusuf. «Prognostic value of heart rate variability in patients with cancer». In: *Journal of clinical neurophysiology: official publication of the American Electroencephalographic Society* 32.6 (2015), p. 516 (cit. on p. 6).

[15] Do Hoon Kim, Jeong A Kim, Youn Seon Choi, Su Hyun Kim, June Young Lee, and Young Eun Kim. «Heart rate variability and length of survival in hospice cancer patients». In: *Journal of Korean Medical Science* 25.8 (2010), pp. 1140–1145 (cit. on p. 6).

[16] Jui-Kun Chiang, Malcolm Koo, Terry BJ Kuo, and Chin-Hua Fu. «Association between cardiovascular autonomic functions and time to death in patients with terminal hepatocellular carcinoma». In: *Journal of pain and symptom management* 39.4 (2010), pp. 673–679 (cit. on p. 6).

[17] Jack A Tuszynski and Frederico Costa. «Low-energy amplitude-modulated radiofrequency electromagnetic fields as a systemic treatment for cancer: Review and proposed mechanisms of action». In: *Frontiers in Medical Technology* 4 (2022), p. 869155 (cit. on pp. 6, 7).

[18] Jacquelyn W Zimmerman, Hugo Jimenez, Michael J Pennison, Ivan Brezovich, Desiree Morgan, Albert Mudry, Frederico P Costa, Alexandre Barbault, and Boris Pasche. «Targeted treatment of cancer with radiofrequency electromagnetic fields amplitude-modulated at tumor-specific frequencies». In: *Chinese journal of cancer* 32.11 (2013), p. 573 (cit. on p. 7).

[19] Fernanda Capareli et al. «Low-energy amplitude-modulated electromagnetic field exposure: Feasibility study in patients with hepatocellular carcinoma». In: *Cancer Medicine* (2023) (cit. on p. 7).

[20] Paul CW Davies, Lloyd Demetrius, and Jack A Tuszynski. «Cancer as a dynamical phase transition». In: *Theoretical Biology and Medical Modelling* 8 (2011), pp. 1–16 (cit. on p. 7).

[21] Zoe Schofield et al. «Bioelectrical understanding and engineering of cell biology». In: *Journal of the Royal Society Interface* 17.166 (2020), p. 20200013 (cit. on p. 7).

[22] Paola Nicolini, Michele M Ciulla, CARLO DE ASMUNDIS, Fabio Magrini, and Pedro Brugada. «The prognostic value of heart rate variability in the elderly, changing the perspective: from sympathovagal balance to chaos theory». In: *Pacing and clinical electrophysiology* 35.5 (2012), pp. 621–637 (cit. on p. 8).

[23] Markad V Kamath and Ernest L Fallen. «Power spectral analysis of heart rate variability: a noninvasive signature of cardiac autonomic function.» In: *Critical reviews in biomedical engineering* 21.3 (1993), pp. 245–311 (cit. on p. 8).

[24] J Thomas Bigger Jr, Richard C Steinman, Linda M Rolnitzky, Joseph L Fleiss, Paul Albrecht, and Richard J Cohen. «Power law behavior of RR-interval variability in healthy middle-aged persons, patients with recent acute myocardial infarction, and patients with heart transplants». In: *Circulation* 93.12 (1996), pp. 2142–2151 (cit. on p. 10).

[25] Robert E Kleiger, Phyllis K Stein, and J Thomas Bigger Jr. «Heart rate variability: measurement and clinical utility». In: *Annals of Noninvasive Electrocardiology* 10.1 (2005), pp. 88–101 (cit. on p. 10).

[26] GG Berntson, JT Cacioppo, M Malik, and AJ Camm. «Dynamic electrocardiography». In: *Future* (2004), pp. 57–64 (cit. on p. 10).

[27] Balth Van Der Pol and Jan Van Der Mark. «LXXII. The heartbeat considered as a relaxation oscillation, and an electrical model of the heart». In: *The London, Edinburgh, and Dublin Philosophical Magazine and Journal of Science* 6.38 (1928), pp. 763–775 (cit. on pp. 11, 12).

[28] T Marios. «Theoretical and Numerical Study of the Van der Pol equation». PhD thesis. Dissertation, 2006 (cit. on p. 12).

[29] Muhammad Asif Zahoor Raja, Fiaz Hussain Shah, and Muhammad Ibrahim Syam. «Intelligent computing approach to solve the nonlinear Van der Pol system for heartbeat model». In: *Neural Computing and Applications* 30 (2018), pp. 3651–3675 (cit. on pp. 14, 28, 37).

[30] Alan Wolf, Jack B Swift, Harry L Swinney, and John A Vastano. «Determining Lyapunov exponents from a time series». In: *Physica D: nonlinear phenomena* 16.3 (1985), pp. 285–317 (cit. on p. 14).

[31] Augusto Cheffer, Marcelo A Savi, Tiago Leite Pereira, and Aline Souza de Paula. «Heart rhythm analysis using a nonlinear dynamics perspective». In: *Applied Mathematical Modelling* 96 (2021), pp. 152–176 (cit. on pp. 15, 16).

[32] Robert Shaw. «Strange attractors, chaotic behavior, and information flow». In: *Zeitschrift für Naturforschung A* 36.1 (1981), pp. 80–112 (cit. on p. 15).

[33] RF Fonkou, Romanic Kengne, Herton Carel Fotsing Kamgang, and PK Talla. «Dynamical behavior analysis of the heart system by the bifurcation structures». In: *Heliyon* 9.1 (2023) (cit. on p. 15).

[34] Mazhar B Tayel and Eslam I AlSaba. «Robust and sensitive method of lyapunov exponent for heart rate variability». In: *arXiv preprint arXiv:1508.00996* (2015) (cit. on p. 16).

[35] Vahid Houshyarifar and Mehdi Chehel Amirani. «Early detection of sudden cardiac death using Poincaré plots and recurrence plot-based features from HRV signals». In: *Turkish Journal of Electrical Engineering and Computer Sciences* 25.2 (2017), pp. 1541–1553 (cit. on p. 17).

[36] Agnieszka Kitlas Golińska. «Poincaré plots in analysis of selected biomedical signals». In: *Studies in logic, grammar and rhetoric* 35.1 (2013), pp. 117–127 (cit. on p. 17).

[37] Otto Frank. *Die grundform des arteriellen pulses: mathematische analyse. erste abhandlung*. 1899 (cit. on p. 18).

[38] Nico Westerhof, Jan-Willem Lankhaar, and Berend E Westerhof. «The arterial windkessel». In: *Medical & biological engineering & computing* 47.2 (2009), pp. 131–141 (cit. on p. 20).

[39] Philipp Broemser and Otto Friedrich Ranke. *Ueber die Messung des Schlagvolumens des Herzens auf unblutigem Weg*. Lehmann, 1930 (cit. on p. 20).

[40] RH Mohiaddin, SR Underwood, HG Bogren, DN Firmin, RH Klipstein, RS Rees, and DB Longmore. «Regional aortic compliance studied by magnetic resonance imaging: the effects of age, training, and coronary artery disease.» In: *Heart* 62.2 (1989), pp. 90–96 (cit. on p. 21).

[41] Yoji Nagai, Jeroen Helwegen, Jerome L Fleg, Mary K Beemer, Christopher J Earley, and E Jeffrey Metter. «Associations of aortic Windkessel function with age, gender and cardiovascular risk factors». In: *Ultrasound in medicine & biology* 27.9 (2001), pp. 1207–1210 (cit. on p. 22).

[42] Gustav G Belz. «Elastic properties and Windkessel function of the human aorta». In: *Cardiovascular drugs and therapy* 9 (1995), pp. 73–83 (cit. on p. 22).

[43] Jay F Piccirillo, Ryan M Tierney, Irene Costas, Lori Grove, and Edward L Spitznagel Jr. «Prognostic importance of comorbidity in a hospital-based cancer registry». In: *Jama* 291.20 (2004), pp. 2441–2447 (cit. on p. 22).

[44] Aristeidis Seretis, Sofia Cividini, Georgios Markozannes, Xanthippi Tseretopoulou, David S Lopez, Evangelia E Ntzani, and Konstantinos K Tsilidis. «Association between blood pressure and risk of cancer development: a systematic review and meta-analysis of observational studies». In: *Scientific reports* 9.1 (2019), p. 8565 (cit. on pp. 22, 23).

[45] Giovanni Corrao, Lorenza Scotti, Vincenzo Bagnardi, and Roberto Sega. «Hypertension, antihypertensive therapy and renal-cell cancer: a meta-analysis». In: *Current drug safety* 2.2 (2007), pp. 125–133 (cit. on p. 22).

[46] Joanne S Colt et al. «Hypertension and risk of renal cell carcinoma among white and black Americans». In: *Epidemiology (Cambridge, Mass.)* 22.6 (2011), p. 797 (cit. on p. 23).

[47] Manuela Gago-Dominguez, J Esteban Castelao, Jian-Min Yuan, Ronald K Ross, and Mimi C Yu. «Lipid peroxidation: a novel and unifying concept of the etiology of renal cell carcinoma (United States)». In: *Cancer Causes & Control* 13 (2002), pp. 287–293 (cit. on p. 23).

[48] Paweł Sobczuk, Cezary Szczylik, Camillo Porta, and Anna M Czarnecka. «Renin angiotensin system deregulation as renal cancer risk factor». In: *Oncology Letters* 14.5 (2017), pp. 5059–5068 (cit. on p. 23).

[49] Elie Mouhayar and Abdulla Salahudeen. «Hypertension in cancer patients». In: *Texas Heart Institute Journal* 38.3 (2011), p. 263 (cit. on p. 23).

[50] Alberto Milan, Elisabetta Puglisi, Laura Ferrari, Giulia Bruno, Isabel Losano, and Franco Veglio. «Arterial hypertension and cancer». In: *International journal of cancer* 134.10 (2014), pp. 2269–2277 (cit. on p. 23).

[51] Babak Nazer, Benjamin D Humphreys, and Javid Moslehi. «Effects of novel angiogenesis inhibitors for the treatment of cancer on the cardiovascular system: focus on hypertension». In: *Circulation* 124.15 (2011), pp. 1687–1691 (cit. on p. 23).

[52] Morihiro Matsuda and Iichiro Shimomura. «Increased oxidative stress in obesity: implications for metabolic syndrome, diabetes, hypertension, dyslipidemia, atherosclerosis, and cancer». In: *Obesity research & clinical practice* 7.5 (2013), e330–e341 (cit. on p. 23).

[53] Goya Wannamethee and AG Shaper. «Blood pressure and cancer in middle-aged British men». In: *International journal of epidemiology* 25.1 (1996), pp. 22–31 (cit. on p. 23).

[54] Krzysztof Grudziński and Jan J Żebrowski. «Modeling cardiac pacemakers with relaxation oscillators». In: *Physica A: statistical Mechanics and its Applications* 336.1-2 (2004), pp. 153–162 (cit. on pp. 28, 29, 32, 60).

[55] Fabián M Lopez-Chamorro, Andrés F Arciniegas-Mejia, David Esteban Imbajoa-Ruiz, Paul D Rosero-Montalvo, Pedro García, Andrés Eduardo Castro-Ospina, Antonio Acosta, and Diego Hernán Peluffo-Ordóñez. «Cardiac pulse modeling using a modified van der pol oscillator and genetic algorithms». In: *Bioinformatics and Biomedical Engineering: 6th International Work-Conference, IWBBIO 2018, Granada, Spain, April 25–27, 2018, Proceedings, Part I 6*. Springer. 2018, pp. 96–106 (cit. on pp. 30, 60).

[56] M Catanho, M Sinha, and V Vijayan. *Model of Aortic Blood Flow using the Windkessel Effect. Report: BENG 221-Mathematical Methods in Bioengineering*. 2012 (cit. on p. 56).

[57] Nicolaas Westerhof, GIJS Elzinga, and Pieter Sipkema. «An artificial arterial system for pumping hearts.» In: *Journal of applied physiology* 31.5 (1971), pp. 776–781 (cit. on p. 57).

[58] Jordi Alastruey, Nan Xiao, Henry Fok, Tobias Schaeffter, and C Alberto Figueroa. «On the impact of modelling assumptions in multi-scale, subject-specific models of aortic haemodynamics». In: *Journal of The Royal Society Interface* 13.119 (2016), p. 20160073 (cit. on p. 63).